Transcription-dependent DNA supercoils determine the 3D organization of dinoflagellate genomes

Georgi K. Marinov[1,,*,#], Alexandro E. Trevino[3,7,*], Tingting Xiang[2,8,*], XXX ADDITIONAL AUTHORS[XX], John R. Pringle[1], Anshul Kundaje[1,6], Arthur R. Grossman[2], and William J. Greenleaf[1,3,4,5,#]

[1] *Department of Genetics, Stanford University, Stanford, California 94305, USA*
[2] *Carnegie Institution for Science, Department of Plant Biology, Stanford, California 94305, USA*
[3] *Center for Personal Dynamic Regulomes, Stanford University, Stanford, California 94305, USA*
[4] *Department of Applied Physics, Stanford University, Stanford, California 94305, USA*
[5] *Chan Zuckerberg Biohub, San Francisco, California, USA*
[6] *Department of Computer Science, Stanford University, Stanford, California 94305, USA*
[7] *Department of Bioengineering, Stanford University, Stanford, California 94305, USA*
[8] *Department of Biological Sciences, University of North Carolina at Charlotte, Charlotte, NC 28223, USA*
[*] *These authors contributed equally to this work*
[#] *Corresponding author*

Abstract

Dinoflagellate chromosomes represent a unique evolutionary experiment within eukaryotes. Their chromosomes exist in a permanently condensed, liquid crystalline state, and are not packaged by nucleosomal histones but rather by proteins of viral and bacterial origin. Genes are organized into polycistronic arrays, and transcriptional regulation is thought to be largely absent. The physical organization of these chromosomes has long remained a mystery. Here, we analyze the 3D genome of *Breviolum minutum*, a coral symbiont dinoflagellate. We find that the genome partitions into large topologically associating domains, not associated with chromatin loops. Domain boundaries instead correspond to transitions between convergent gene arrays. Transcriptional inhibition degrades these domains, implicating transcription-induced supercoiling as a primary topological force in dinoflagellate chromatin and torsional stress as a fundamental force that must be accommodated by all organisms.

Recent investigations into the three-dimensional organization of genomes and its functional consequences in mammalian systems have identified multiple physical mechanisms underlying genome folding (2). Two main topological forces are currently thought to drive 3D organization. Associations between similar chromatin states drive the formation of compartments, and this mechanism is probably present in most eukaryotes (2). Better known (and more prominent in mammalian genomes) are the constraints on cohesin-mediated loop extrusion (3), imposed by pairs of boundary elements specified by occupancy sites of the CTCF insulation factor. They drive the formation of topologically associating loop extrusion domains (TADs), approximately 100-1000 kbp in size (3).

Three-dimensional genome architecture has been proposed to have multiple important functional consequences for gene regulation (4, 5), organismal development (6), replication (7), mutational processes (8), and others. However, how functional activity in turn impacts genome organization is still poorly understood. There has also been relatively little exploration of how these biophysical properties vary across eukaryotes even though several groups exhibit major deviations from conventional eukaryotic norms, thus presenting natural experiments that may reveal deeper underlying principles of genome organization that are masked in other lineages.

Dinoflagellates are the most radical such departure. They are a diverse, widespread lineage of eukaryotes that play major roles in aquatic ecosystems. As an example, the association of dinoflagellates in the Symbiodiniaceae clade (9) with reef-building coral species provides the metabolic basis for vital and highly biologically diverse reef ecosystems. They are also a unique lineage possessing numerous highly divergent molecular features (10), including the striking fact that the fundamental unit of chromatin organization is not the nucleosome. Nucleosomal packaging of

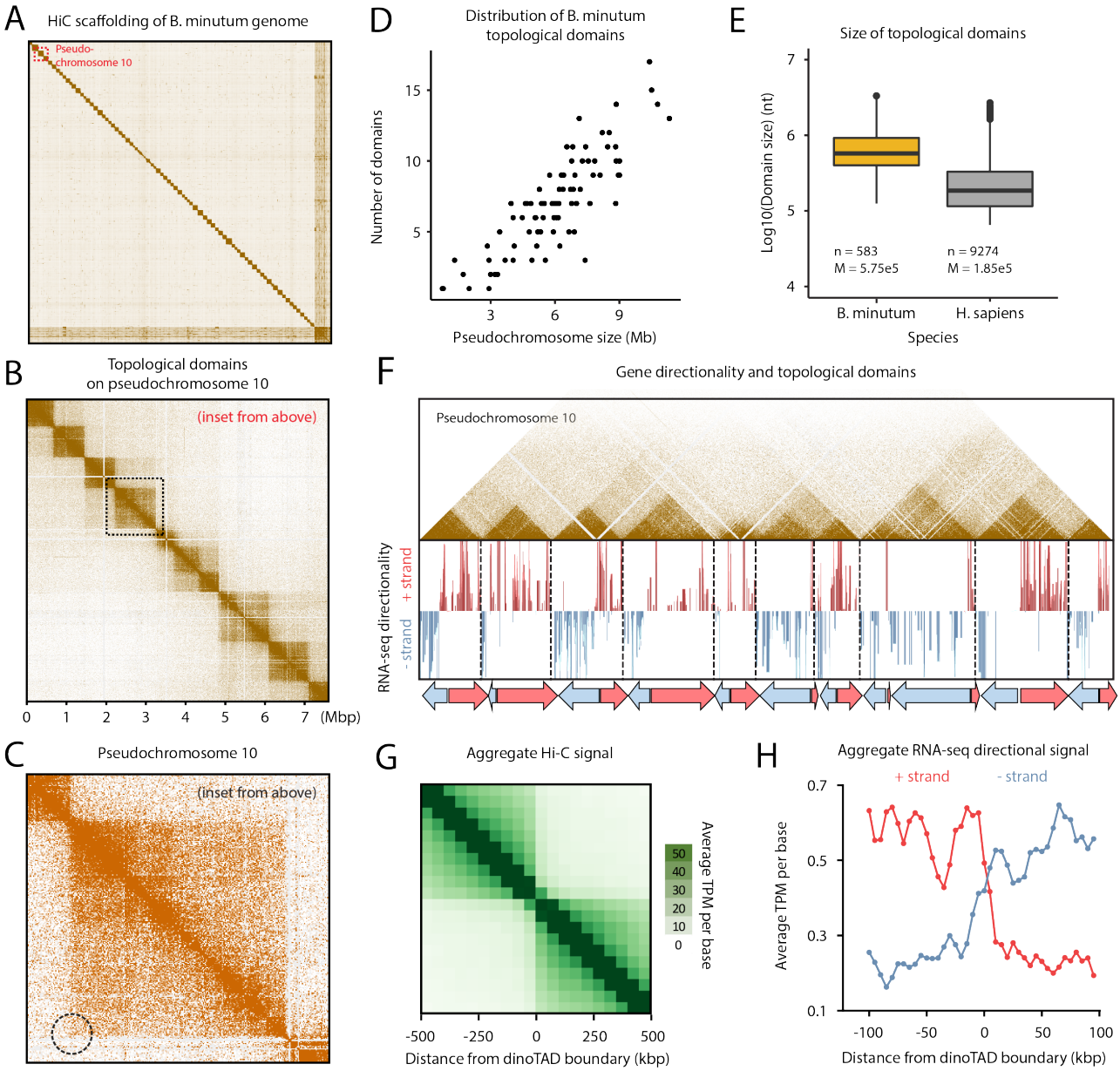

Figure 1: *B. minutum* genome is physically partitioned into topological domains defined by polycistronic gene arrays. (A-C) Organization of dinoflagellate chromosomes. (A) Hi-C scaffolding of the *B. minutum* draft genome assembly identifies 91 major pseudochromosomes ≥500kb in size. (B) Inset from (A). KR-normalized (1) 5-kb resolution Hi-C map for pseudochromosome 10. Pseudochromosomes are physically partitioned into strong topological domains ("dinoTADs"). (C) Focus on a single topological domain, inset from (D). The usual signs of loop extrusion domains (presence of loops and stripes in Hi-C maps) are not observed in dinoTADs. (D) The number of dinoTADs per chromosome scales with chromosome size. (E) Comparison of *H. sapiens* (grey) and *B. minutum* (yellow) topological domain sizes. (F-H) Boundaries of dinoTADs are primarily associated with transitions between convergent polycistronic gene arrays. (F) Shown is the Hi-C map for pseudochromosome 10 together with transcript levels on the forward and the reverse strands. (G) Average Hi-C contacts across dinoTAD boundaries. (H) Average forward- and reverse-strand RNA-seq contacts across dinoTAD boundaries.

chromatin evolved in archaea and developed into its present form prior to the time of the Last Eukaryotic Common Ancestor (LECA) (11). All living eukaryotes ancestrally possess four core nucleosomal histones (H2A, H2B, H3 and H4), each featuring long unstructured N-terminal tails. These tails, as well as a few residues in the histone fold domain, are subject to extensive posttranslational modifications, forming the basis of the so called "histone code" (12) and playing

important roles in essentially all biochemical processes involving chromatin. Its fundamental importance is strongly underscored by the fact that key histone code residues are almost invariant across eukaryotes (13).

Dinoflagellates are the sole known exception. Their chromosomes exist in a liquid crystalline state, are permanently condensed throughout the cell cycle, and are characterized by a very low DNA to protein ratio of 1:10 (compared to the usual 1:1 (14)). This is because, even though histone genes (although highly divergent) are retained in dinoflagellate genomes (15), a combination of virus-derived dinoflagellate-specific nucleoproteins (DVNPs) and bacterial-derived histone-like proteins (HLPs) have taken over as the main DNA packaging components (16, 17).

The functional organization of dinoflagellate genomes is also unusual, though not without some parallels (18), as genes are organized into polycistronic gene arrays transcribed as a single unit, with individual mRNAs generated through *trans*-splicing; it is generally thought that transcriptional regulation is largely absent. In addition, despite being relatively small unicellular organisms, their genomes are often very large in size (up to 100-fold larger than mammalian genomes).

These fascinating features of dinoflagellate nuclei simultaneously present numerous intriguing questions regarding the adaptation of the conventional eukaryotic gene regulation mechanisms to the general absence of nucleosomal chromatin, and also provide an opportunity to explore the biophysical forces underlying genomic organization in a large eukaryotic genome in the absence of nucleosomes.

Here, we chart the 3D genome of the coral symbiont *Breviolum minutum* (previously *Symbiodinium minutum*), and uncover a novel mechanism for its organization.

We first generated three genome-wide chromosome conformation capture (Hi-C) libraries for the *B. minutum* SSB01 strain using a slight modification of the standard *in situ* Hi-C protocol (3), including one under elevated temperature conditions. We obtained between ∼150 and 220 million distinct Hi-C contacts from each library (Supplementary Table 1). We pooled reads from all samples and processed them against the existing, highly fragmented *B. minutum* assembly (19), then used the resulting Hi-C maps to generate a chromosome-level assembly scaffolding using established methods (20) (see Supplementary Methods for details). The resulting assembly consists of 91 major pseudochromosomes ≥ 500 kbp in size, encompassing ∼94% of the total sequence, with 85 of them ≥1 Mbp (Figure 1A, B and Supplementary Figure 1 A). The longest major pseudochromosomes are ∼11 Mbp in size, with a median length of 6.7 Mbp (Supplementary Figure 1A). At 1-Mbp resolution, they exhibit a bipartite (on a few occasions tripartite) structure, with two major interacting domains (Supplementary Figure 2).

This assembly underestimates the total genome size, as the original set of contigs clearly contains a number of collapsed repeats, which is common feature of Hi-C-based genome assemblies (Figure 1A, lower right). While previous reports suggest the existence of ∼20 chromosomes based on microscopy images (19), Hi-C analysis strongly suggests the physical separation of a larger number of pseudochromosomes in the nucleus, as does the recent chromosome-level assembly of *F. kawagutii* (another Symbiodiniaceae species) (21).

High-resolution (5 kbp) maps revealed the existence of strong topological domains ranging in length from ≤ 200 kbp to ≥2 Mbp (Figure 1B-E, Supplementary Figures 3–12). In mammals, where TADs are best documented (3), TAD boundaries are demarcated by opposite-orientation pairs of CTCF sites that block loop extrusion by cohesin rings (2). Constraints on loop extrusion are reflected in high-resolution Hi-C maps by the presence of loops at TAD boundaries and "stripes" on the edges of TAD blocks (5). In contrast, we observed no loop or stripe features in *B. minutum* (Figure 1C), suggesting that dinoflagellate TADs are formed by a different mechanism. We term these domains "dinoTADs" to distinguish them from the loop extrusion-related domains in vertebrates. The number of dinoTADs appears to be a function of the chromosome size (Figure 1D), while comparison with mammalian TADs reveals dinoTADs to be considerably larger (Figure 1E).

In order to understand the formation of dinoTADs, we compared Hi-C maps to available annotation features for *B. minutum*, in particular transcriptomic data (Supplementary Methods). Remarkably, we found that each dinoTAD corresponds to a pair of divergent gene arrays (Figure 1F), while boundaries between dinoTADs coincide with regions of convergence between gene arrays (Figure 1G-H).

Numerous models for dinoflagellate chromosome organization have been suggested since the 1960s, primarily based on electron microscopy. These include proposals that chromosomes are organized as "toroidal chromonemas" (23), "stacks of discs" (24), "cored pineapples" (25), or around "central core fibers" (26). Most of these models imply specific topological constraints maintaining the proposed shapes.

The Hi-C patterns we observe do not immediately fit with these models, and instead strongly suggest a role for dynamic transcription-dependent DNA supercoiling in dinoTAD formation. Studies of 3D genome organization in bacteria have suggested that transcription can cause the formation of self-interacting domains (27), and similar mechanisms have been proposed as an explanation for topological features observed in the yeast *Schizosaccharomyces pombe* (28). Transcription can affect topological features due to its effects on DNA supercoiling (29) – the torque generated by RNA polymerase causes positive supercoiling in front of the transcription bubble and negative supercoiling behind it. The resulting torsional stress triggers changes in DNA shape by altering the twist of the double helix or inducing superhelical writhe, which could in turn be accommodated though the formation of plectonemes, nucleosome remodeling, or others alterations in DNA structure (30).

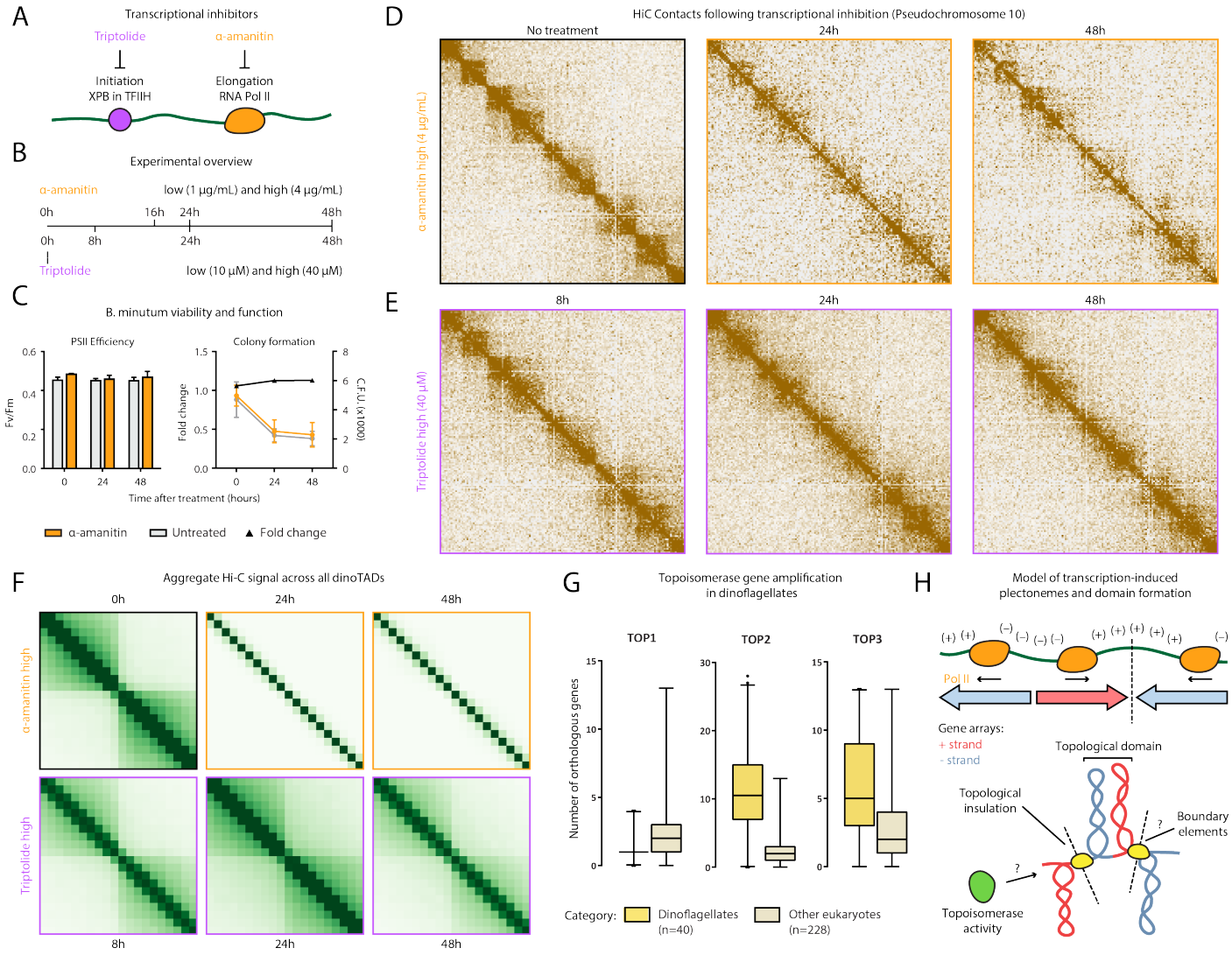

Figure 2: Decompaction of dinoTADs upon transcriptional inhibition supports the transcription-induced supercoiling model for their formation. Shown is pseudochromosome 10 as in Figure 1. (A) Outline of transcription inhibition experiments carried out using α-amanitin (orange) and triptolide (purple). (B) Time course and dosages of transcriptional inhibition. (C) Comparison of cell function, measured by PSII photosythetic efficiency test (left), and cell viability, measured by a colony counting assay (right), between α-amanitin-treated and untreated samples over time. (D) KR-normalized Hi-C maps (50-kb resolution) at 0 hours, 24 hours and 48 hours (high dose) after α-amanitin treatment show marked loss of dinoTADs. (E) KR-normalized Hi-C maps (50-kb resolution) at 8 hours, 24 hours and 48 hours (high dose) after triptolide treatment show reduction of insulation at dinoTAD boundaries. (F) Metaplots of Hi-C signal around domain boundaries (50-kb resolution; see Supplementary Methods for details). (G) Amplification of *TOP2* and *TOP3* topoisomerase homolog genes in dinoflagellates compated to other unicellular eukaryotes. Transcriptome assemblies from the MMETSP (22) were used (See Supplementary Methods for details). (H) Transcription-induced supercoiling as the main topological force driving the physical organization of dinoflagellate chromosomes. Transcribing RNA Polymerase molecules introduce negative and positive DNA supercoling behind and ahead of the transcription machinery, respectively, and the interactions of negatively supercoiled domains could explain the physical association of divergently-oriented gene arrays. Topological insulation could be driven by supercoiling-related effects, or by unknown boundary elements. Also unknown at present is the role of the expanded repertoire of topoisomerases.

Transcription-driven plectoneme formation coinciding with long dinoflagellate gene arrays is an intuitive explanation for the compact dinoTADs we observe, although it is also possible that other topological constraints are involved.

The transcription-induced supercoiling model makes a clear prediction that can distinguish these possibilities – in-

hibition of transcription should lead to the decompaction of dinoTADs.

We first compared Hi-C maps for *B. minutum* cells grown at 27 °C and at 34 °C, as exposure to heat stress could result in general reduction in transcription activity (31). Indeed, while we do not observe disappearance of dinoTADs in the 34 °C sample, we do observe mild dinoTAD decompaction and an increase in interactions across dinoTAD boundaries (Supplementary Figures 18–20).

To test the transcription-induced supercoiling model, we carried out transcription inhibition experiments using α-amanitin and triptolide (Figure 2A-B). Triptolide prevents transcription initiation by targeting the XPB subunit of the TFIIH complex, and is fast acting (within hours). In contract, α-amanitin directly inhibits RNA Polymerase II, and usually takes $\geq$12 hours to act due to its slow uptake by cells (32). We note that well-established transcription inhibition conditions for *B. minutum* are lacking, and it is quite possible that inhibitor uptake is more difficult than in mammalian cells. It is also possible that triptolide does not strongly inhibit transcription due to the divergence of dinoflagellate transcription machinery components. We therefore carried out two sets of experiments, one using a "normal" dose for each inhibitor (the one usually used for mammalian cells) and a "high" dose (4× higher), harvesting cells at 0, 8, 24 and 48 hours for triptolide and at 0, 16, 24 and 48 hours for α-amanitin.

Of note, we found that even a high concentration of 4 μg/mL α-amanitin did not cause detectable decreases in photosynthetic efficiency or cell viability relative to untreated controls (Figure 2C), thus excluding increased cell death as a confounding factor in our analysis.

Strikingly, treatment with α-amanitin resulted in a dose-dependent progressive, near-complete disappearance of dinoTADs over 48 hours (Figure 2D and F; Supplementary Figures 21–24). Triptolide treatment did not trigger a disappearance of all topological structures, but nevertheless induced "blurring" of boundaries between dinoTADs (Figure 2E-F; Supplementary Figures 25–28); this milder effect, as mentioned above, is possibly the result of XPB protein divergence (19). The effects of transcriptional inhibition were observed in both technical and biological replicates (Supplementary Figures 21–24), and on aggregate across all dinoTADs (Figure 2F).

Taken together, these observations support transcription-driven supercoiling as the primary force driving the formation of dinoTADs. Examination of dinoflagellate gene repertoires also suggests that their genomes contend with elevated torsional stress. We surveyed available transcriptome assemblies for dinoflagellates and a wide sampling of other unicellular eukaryotes (22) and uncovered a striking expansion of topoisomerase II- and topoisomerase III-like genes (but not topoisomerase I-like genes) within dinoflagellates (Figure 1D; Supplementary Figure 17; Supplementary Table 2); topoisomerases are necessary for relieving transcription-induced torsional stress (33).

Comparison of dinoflagellate Hi-C data to that from other organisms shows that topological insulation within dinoTADs is much stronger than self-interacting domains observed in bacteria or *S. pombe* (Supplementary Figures 14) and 15)), and that no such domains are observed in Hi-C datasets for kinetoplastids, the other well-known lineage of eukaryotes with highly prominent unidirectional polycistronic gene arrays and loss of transcription-level gene regulation (Supplementary Figures 16). These differences are readily explained as the result of the unusual properties of dinoflagellates.

Neither bacteria nor *S. pombe* possess unidirectional gene arrays of length comparable to that of dinoflagellates; furthermore, transcription is also highly nonuniform across the genome. Accordingly, the amount of transcription-induced torsional stress is expected to be reduced.

The general absence of nucleosomes is the second, and likely most salient difference. In mammals, where genes as long as dinoTADs are quite common (due to the presence of extremely long introns), transcription-dependent DNA supercoiling is not directly apparent as a topological force in Hi-C maps, nor is it seen in kinetoplastids, which lack transcriptional regulation and have long gene arrays, but have conventional nucleosomal chromatin. Thus we hypothesize that transcription-induced plectonemes are free to form in dinoflagellate genomes due to the lack of nucleosomes, but may be highly constrained in other eukaryotes, where interactions between nucleosomes may it energetically costly to form writhe-based structures like plectonemes, requiring more of this torsion to be taken up by changes in DNA twist (Figure 2H).

In summary, we have presented the first map of the physical organization of a dinoflagellate genome using modern molecular tools and have found unexpected links to the functional organization of the genome. The folding of the dinoflagellate genome in 3D space appears to be primarily dependent on transcription, which drives transcription-dependent DNA supercoiling. This model is supported by the co-association of topological domains with the boundaries between divergent gene array pairs, the large expansion of topoisomerase genes in dinoflagellate genomes, and the disappearance of dinoTADs upon exposure to general inhibitors of transcription. As the only known eukaryotes that do not use histones to package DNA, dinoflagellates represent a unique evolutionary experiment that reveals aspects of genome biology that are otherwise masked by nucleosomal chromatin and insulation. This natural experiment also highlights the potential magnitude of transcription-induced supercoiling as a general organizing force for genomes given that transcription-induced torsional stress is present in all organisms.

A number of open questions remain. It is possible that as-yet unidentified functional boundary elements of markedly different chromatin state exist at the boundaries of gene arrays; it is also currently unclear what exactly role histones play in dinoflagellate genomes. Answers to these

questions, together with understanding the specific actions and genomic localization of the large repertoire of topoisomerase enzymes, will be critical for fully clarifying the interplay between nucleosomes, other packaging proteins, torsional stress and genome folding in dinoflagellates.

Our results also point to transcription-induced torsional stress as a key direction of future studies even in conventional eukaryotes. The strength of dinoTADs underlines the fact that transcription-generated torsion can be a potent topological force shaping chromatin organization. How is this torsional stress accommodated in other eukaryotes? While we have suggested that interactions between nucleosomes likely prevent torsion from translating into large plectonemes, and others have suggested that chromatin fibers may act as a torsional twist buffer (34), the precise manner by which transcription-induced torsion is accommodated as twist and writhe in mammalian genomes, as well as its consequences for regulatory protein occupancy, transcriptional activity and other chromatin processes are exciting question remaining to be unraveled.

Author contributions

G.K.M. performed Hi-C experiments. G.K.M and A.E.T. analyzed the data. A.E.T. and T.X. carried out transcription inhibition experiments and cell viability experiments. T.X. carried out *S. minutum* culture and heat stress treatment. W.J.G., A.R.G.. A.K. and J.R.P. supervised the study. G.K.M., A.E.T. and T.X. interpreted data and wrote manuscript with input from all authors.

Acknowledgments

This work was supported by NIH grants (P50HG007735, RO1 HG008140, U19AI057266 and UM1HG009442 to W.J.G., 1UM1HG009436 to W.J.G. and A.K., 1DP2OD022870-01 and 1U01HG009431 to A.K.), the Rita Allen Foundation (to W.J.G.), the Baxter Foundation Faculty Scholar Grant, and the Human Frontiers Science Program grant RGY006S (to W.J.G). W.J.G is a Chan Zuckerberg Biohub investigator and acknowledges grants 2017-174468 and 2018-182817 from the Chan Zuckerberg Initiative. Fellowship support provided by the Stanford School of Medicine Dean's Fellowship (G.K.M.), the Siebel Scholars, the Enhancing Diversity in Graduate Education Program and the Weiland Family Fellowship (A.E.T.). This work is also supported by NSF-IOS EDGE Award 1645164 and Carnegie Venture grant 10907 (to T.X. and G.K.M.).

The authors would like to thank Zohar Shipony, Erez Lieberman Aiden, Philip Cleves, and members of the Greenleaf, Kundaje, Pringle and Grossman labs for helpful discussion and suggestions regarding this work.

References

1. Knight P, Ruiz D. 2013. A fast algorithm for matrix balancing. *IMA J Num Anal* **33**(3):1029–1047.
2. Szabo Q, Bantignies F, Cavalli G. 2019. Principles of genome folding into topologically associating domains. *Sci Adv* **5**(4):eaaw1668.
3. Rao SSP, Huang SC, Glenn St Hilaire B, Engreitz JM, Perez EM, Kieffer-Kwon KR, Sanborn AL, Johnstone SE, Bascom GD, Bochkov ID, Huang X, Shamim MS, Shin J, Turner D, Ye Z, Omer AD, Robinson JT, Schlick T, Bernstein BE, Casellas R, Lander ES, Aiden EL. 2017. Cohesin Loss Eliminates All Loop Domains. *Cell* **171**(2):305–320.e24.
4. Narendra V, Rocha PP, An D, Raviram R, Skok JA, Mazzoni EO, Reinberg D. 2015. CTCF establishes discrete functional chromatin domains at the *Hox* clusters during differentiation. *Science* **347**(6225):1017–1021.
5. Vian L, Pekowska A, Rao SSP, Kieffer–Kwon KR, Jung S, Baranello L, Huang SC, El Khattabi L, Dose M, Pruett N, Sanborn AL, Canela A, Maman Y, Oksanen A, Resch W, Li X, Lee B, Kovalchuk AL, Tang Z, Nelson S, Di Pierro M, Cheng RR, Machol I, St Hilaire BG, Durand NC, Shamim MS, Stamenova EK, Onuchic JN, Ruan Y, Nussenzweig A, Levens D, Aiden EL, Casellas R. 2018. The Energetics and Physiological Impact of Cohesin Extrusion. *Cell* **173**(5):1165–1178.e20.
6. Lupiáñez DG, Kraft K, Heinrich V, Krawitz P, Brancati F, Klopocki E, Horn D, Kayserili H, Opitz JM, Laxova R, Santos-Simarro F, Gilbert-Dussardier B, Wittler L, Borschiwer M, Haas SA, Osterwalder M, Franke M, Timmermann B, Hecht J, Spielmann M, Visel A, Mundlos S. 2015. Disruptions of topological chromatin domains cause pathogenic rewiring of gene-enhancer interactions. *Cell* **161**(5):1012–1025.
7. Pope BD, Ryba T, Dileep V, Yue F, Wu W, Denas O, Vera DL, Wang Y, Hansen RS, Canfield TK, Thurman RE, Cheng Y, Gülsoy G, Dennis JH, Snyder MP, Stamatoyannopoulos JA, Taylor J, Hardison RC, Kahveci T, Ren B, Gilbert DM. 2014. Topologically associating domains are stable units of replication-timing regulation. *Nature* **515**(7527):402–405.
8. Canela A, Maman Y, Jung S, Wong N, Callen E, Day A, Kieffer-Kwon KR, Pekowska A, Zhang H, Rao SSP, Huang SC, Mckinnon PJ, Aplan PD, Pommier Y, Aiden EL, Casellas R, Nussenzweig A. 2017. Genome Organization Drives Chromosome Fragility. *Cell* **170**(3):507–521.e18.
9. LaJeunesse TC, Parkinson JE, Gabrielson PW, Jeong HJ, Reimer JD, Voolstra CR, Santos SR. 2018. Systematic Revision of Symbiodiniaceae Highlights the Antiquity and Diversity of Coral Endosymbionts. *Curr Biol* **28**(16):2570–2580.e6.
10. Hackett JD, Anderson DM, Erdner DL, Bhattacharya

D. 2004. Dinoflagellates: a remarkable evolutionary experiment. *Am J Bot* **91**:1523–1534.
11. Talbert PB, Meers MP, Henikoff S. 2019. Old cogs, new tricks: the evolution of gene expression in a chromatin context. *Nat Rev Genet* **20**(5):283–297.
12. Jenuwein T, Allis CD. 2001. Translating the histone code. *Science* **293**(5532):1074–1080.
13. Postberg J, Forcob S, Chang WJ, Lipps HJ. 2010. The evolutionary history of histone H3 suggests a deep eukaryotic root of chromatin modifying mechanisms. *BMC Evol Biol* **10**:259.
14. Herzog M, Soyer MO. 1981. Distinctive features of dinoflagellate chromatin. Absence of nucleosomes in a primitive species *Prorocentrum micans* E. *Eur J Cell Biol* **23**(2):295–302.
15. Marinov GK, Lynch M. 2015. Diversity and Divergence of Dinoflagellate Histone Proteins. *G3 (Bethesda)* **6**(2):397–422.
16. Gornik SG, Ford KL, Mulhern TD, Bacic A, McFadden GI, Waller RF. 2012. Loss of nucleosomal DNA condensation coincides with appearance of a novel nuclear protein in dinoflagellates. *Curr Biol* **22**(24):2303–2312.
17. Janouškovec J, Gavelis GS, Burki F, Dinh D, Bachvaroff TR, Gornik SG, Bright KJ, Imanian B, Strom SL, Delwiche CF, Waller RF, Fensome RA, Leander BS, Rohwer FL, Saldarriaga JF. 2017. Major transitions in dinoflagellate evolution unveiled by phylotranscriptomics. *Proc Natl Acad Sci U S A* **114**(2):E171–E180.
18. Lukes J, Leander BS, Keeling PJ. 2009. Cascades of convergent evolution: the corresponding evolutionary histories of euglenozoans and dinoflagellates. *Proc Natl Acad Sci U S A* **106** Suppl 1:9963–9970
19. Shoguchi E, Shinzato C, Kawashima T, Gyoja F, Mungpakdee S, Koyanagi R, Takeuchi T, Hisata K, Tanaka M, Fujiwara M, Hamada M, Seidi A, Fujie M, Usami T, Goto H, Yamasaki S, Arakaki N, Suzuki Y, Sugano S, Toyoda A, Kuroki Y, Fujiyama A, Medina M, Coffroth MA, Bhattacharya D, Satoh N. 2013. Draft assembly of the *Symbiodinium minutum* nuclear genome reveals dinoflagellate gene structure. *Curr Biol* **23**(15):1399–1408.
20. Dudchenko O, Batra SS, Omer AD, Nyquist SK, Hoeger M, Durand NC, Shamim MS, Machol I, Lander ES, Aiden AP, Aiden EL. 2017. De novo assembly of the Aedes aegypti genome using Hi-C yields chromosome-length scaffolds. *Science* **356**(6333):92–95.
21. Li T, Yu L, Song B, Song Y, Li L, Lin X, Lin S. 2020. Genome Improvement and Core Gene Set Refinement of *Fugacium kawagutii*. *Microorganisms* **8**(1). pii: E102.
22. Keeling PJ, Burki F, Wilcox HM, Allam B, Allen EE, Amaral-Zettler LA, Armbrust EV, Archibald JM, Bharti AK, Bell CJ, Beszteri B, Bidle KD, Cameron CT, Campbell L, Caron DA, Cattolico RA, Collier JL, Coyne K, Davy SK, Deschamps P, Dyhrman ST, Edvardsen B, Gates RD, Gobler CJ, Greenwood SJ, Guida SM, Jacobi JL, Jakobsen KS, James ER, Jenkins B, John U, Johnson MD, Juhl AR, Kamp A, Katz LA, Kiene R, Kudryavtsev A, Leander BS, Lin S, Lovejoy C, Lynn D, Marchetti A, McManus G, Nedelcu AM, Menden-Deuer S, Miceli C, Mock T, Montresor M, Moran MA, Murray S, Nadathur G, Nagai S, Ngam PB, Palenik B, Pawlowski J, Petroni G, Piganeau G, Posewitz MC, Rengefors K, Romano G, Rumpho ME, Rynearson T, Schilling KB, Schroeder DC, Simpson AG, Slamovits CH, Smith DR, Smith GJ, Smith SR, Sosik HM, Stief P, Theriot E, Twary SN, Umale PE, Vaulot D, Wawrik B, Wheeler GL, Wilson WH, Xu Y, Zingone A, Worden AZ. 2014. The Marine Microbial Eukaryote Transcriptome Sequencing Project (MMETSP): illuminating the functional diversity of eukaryotic life in the oceans through transcriptome sequencing. *PLoS Biol* **12**(6):e1001889.
23. Oakley BR. Dodge JD. 1979. Evidence for a double-helically coiled toroidal chromonema in the dinoflagellate chromosome. *Chromosoma* **70**:277–291.
24. Livolant F, Bouligand, Y. 1978. New observations on the twisted arrangement of dinoflagellate chromosomes. *Chromosoma* **68**:21–44.
25. Levi-Setti R, Gavrilov KL, Rizzo PJ. 2008. Divalent cation distribution in dinoflagellate chromosomes imaged by high-resolution ion probe mass spectrometry. *Eur J Cell Biol* **87**(12):963–976.
26. Spector DL, Triemer RE. 1981. Chromosome structure and mitosis in the dinoflagellates: an ultrastructural approach to an evolutionary problem. *Biosystems* **14**(3–4):289–298.
27. Le TB, Imakaev MV, Mirny LA, Laub MT. 2013. High-resolution mapping of the spatial organization of a bacterial chromosome. *Science* **342**(6159):731–734.
28. Benedetti F, Racko D, Dorier J, Burnier Y, Stasiak A. 2017. Transcription-induced supercoiling explains formation of self-interacting chromatin domains in *S. pombe*. *Nucleic Acids Res* **45**(17):9850–9859.
29. Wu HY, Shyy SH, Wang JC, Liu LF. 1988. Transcription generates positively and negatively supercoiled domains in the template. *Cell* **53**(3):433–440.
30. Teves SS, Henikoff S. 2014. DNA torsion as a feedback mediator of transcription and chromatin dynamics. *Nucleus* **5**(3):211–218.
31. Levin RA, Beltran VH, Hill R, Kjelleberg S, McDougald D, Steinberg PD, van Oppen MJ. 2016. Sex, Scavengers, and Chaperones: Transcriptome Secrets of Divergent Symbiodinium Thermal Tolerances. *Mol Biol Evol* **33**(9):2201–2215.
32. Bensaude O. 2011. Inhibiting eukaryotic transcription: Which compound to choose? How to evaluate its activity? *Transcription* **2**(3):103–108.
33. Pommier Y, Sun Y, Huang SN, Nitiss JL. 2016. Roles

of eukaryotic topoisomerases in transcription, replication and genomic stability. *Nat Rev Mol Cell Biol* **17**(11):703–721.
34. Kaczmarczyk A, Meng H, Ordu O, Noort JV, Dekker NH. 2020. Chromatin fibers stabilize nucleosomes under torsional stress. *Nat Commun* **11**(1):126.
35. Xiang T, Hambleton EA, DeNofrio JC, Pringle JR, Grossman AR. 2013. Isolation of clonal axenic strains of the symbiotic dinoflagellate *Symbiodinium* and their growth and host specificity. *J Phycol* **49**(3):447–458.
36. Xiang T, Nelson W, Rodriguez J, Tolleter D, Grossman AR. 2015. *Symbiodinium* transcriptome and global responses of cells to immediate changes in light intensity when grown under autotrophic or mixotrophic conditions. *Plant J* **82**(1):67–80.
37. Mumbach MR, Rubin AJ, Flynn RA, Dai C, Khavari PA, Greenleaf WJ, Chang HY. 2016. HiChIP: efficient and sensitive analysis of protein-directed genome architecture. *Nat Methods* **13**(11):919–922.
38. Durand NC, Shamim MS, Machol I, Rao SS, Huntley MH, Lander ES, Aiden EL. 2016. Juicer Provides a One-Click System for Analyzing Loop-Resolution Hi-C Experiments. *Cell Syst* **3**(1):95–98.
39. Dobin A, Davis CA, Schlesinger F, Drenkow J, Zaleski C, Jha S, Batut P, Chaisson M, Gingeras TR. 2013. STAR: ultrafast universal RNA-seq aligner. *Bioinformatics* **29**(1):15–21.
40. Pertea M, Pertea GM, Antonescu CM, Chang TC, Mendell JT, Salzberg SL. 2015. StringTie enables improved reconstruction of a transcriptome from RNA-seq reads. *Nat Biotechnol* **33**(3):290-295.
41. Eddy SR. 2011. Accelerated Profile HMM Searches. *PLoS Comput Biol* **7**(10):e1002195.
42. Finn RD, Bateman A, Clements J, Coggill P, Eberhardt RY, Eddy SR, Heger A, Hetherington K, Holm L, Mistry J, Sonnhammer EL, Tate J, Punta M. 2014. Pfam: the protein families database. *Nucleic Acids Res* **42**(Database issue):D222–230.

Supplementary Materials

Supplementary Methods

Except where otherwise stated, computational analyses were carried out using custom-written Python scripts.

B. minutum cell culture

The clonal axenic *Symbiodinium/Breviolum minutum* strain SSB01 was used in all experiments. Stock cultures were grown as previously described(35, 36) in Daigo's IMK medium for marine microalgae (Wako Pure Chemicals) supplemented with casein hydrolysate (IMK+Cas) at 27 °C at a light intensity of 10 μmol photons m^2 s^1 from Philips ALTO II 25-W bulbs on a 12-h-light:12-h-dark cycle. The medium was prepared in artificial seawater (ASW).

Transcription inhibition experiments

For α-amanitin treatment, *Breviolum minutum* cells at a density of $\sim$1 $\times 10^6$ cells/mL were treated with α-amanitin (Sigma-Aldrich, Cat # A2263) at concentrations of 1 μg/mL ("normal" dose) and 4 μg/mL ("high") dose.

Samples were harvested at 0, 24, and 48 hours after treatment.

For triptolide treatment, *Breviolum minutum* cells at a density of $\sim$1 $\times 10^6$ cells/mL were treated with triptolide (Sigma-Aldrich, Cat # T3652) at concentrations of 10 μM ("normal" dose) and 40 μM ("high") dose.

Samples were harvested fat 0, 8, 24 and 48 hours after treatment.

Cell viability measurements

Photosynthetic activity

Maximum quantum yields of photosystem II, $Fv/Fm = (Fm - F0)/Fm$ was used to indicate photosynthetic function. S. minutum cultures (approximately 10^6 cells/mL) were collected and dark adapted for 5 min, and Fv/Fm was determined using a Dual Pam-100 fluorometer (Heinz Walz).

Colony formation assay

Fresh SSB01 cells were sampled at 0, 24 and 48 hours after the treatment of transcription inhibitor α-amanitin. For each condition, cell suspensions were diluted 1:5 and 1:10 before plating 1 μL of each dilution on marine broth (BD) agar plates. Plates were incubated at 27 °C at a light intensity of 10 μmol photons m^2 s^1. Cell numbers on each plate were counted after three weeks.

Hi-C experiments

The in situ Hi-C procedure used to map 3D genomic interactions in *Symbiodinium* was adapted from previous studies(3, 37) as follows:

Symbiodinium minutum SSBO1 cells were first crosslinked using 37% formaldehyde (Sigma) at a final concentration of 1% for 15 minutes at room temperature. Formaldehyde was then quenched using 2.5 M Glycine at a final concentration of 0.25 M. Cells were subsequently centrifuged at 2,000 *g* for 5 minutes, washed once in 1× PBS, and stored at -80 °C.

Cell lysis was initiated by incubation with 250 μL of cold Hi-C Lysis Buffer (10 mM Tris-HCl pH 8.0, 10 mM NaCl, 0.2% Igepal CA630) on ice for 15 minutes, followed by centrifugation at 2,500 *g* for 5 minutes, a wash with 500 μL of cold Hi-C Lysis Buffer, and centrifugation at 2,500 *g* for 5 minutes. The pellet was the resuspended in 50 μL of 0.5% SDS and incubated at 62 °C for 10 minutes. SDS was quenched by adding 145 μL of H_2O and 25 μL of 10% Triton X-100 and incubating at 37 °C for 15 minutes.

Restriction digestion was carried out by adding 25 μL of 10× NEBuffer 2 and 100 U of the MboI restriction enzyme (NEB, R0147) and incubating for $\geq$2 hours at 37 °C in a Thermomixer at 900 rpm. The reaction was then incubated at 62 °C for 20 minutes in order to inactivate the restriction enzyme.

Fragment ends were filled in by adding 37.5 μL of 0.4 mM biotin-14-dATP (ThermoFisher Scientific, # 19524-016), 1.5 μL each of 10 mM dCTP, dGTP and dTTP, and 8 μL of 5U/μL DNA Polymerase I Large (Klenow) Fragment (NEB M0210). The reaction was the incubated at 37 °C in a Thermomixer at 900 rpm for 45 minutes.

Fragment end ligation was carried out by adding 663 μL H_2O, 120 μL 10× NEB T4 DNA ligase buffer (NEB B0202), 100 μL of 10% Triton X-100, 12 μL of 10 mg/mL Bovine Serum Albumin (100× BSA, NEB), 5 μL of 400 U/μL T4 DNA Ligase (NEB M0202), and incubating at room temperature for $\geq$4 hours with rotation.

Nuclei were then pelleted by centrifugation at 3,500 *g* for 5 minutes; the pellet was resuspended in 200 μL ChIP Elution Buffer (1% SDS, 0.1 M $NaHCO_3$), Proteinase K was added, and incubated at 65 °C overnight to reverse crosslinks.

After addition of 600 μL 1×TE buffer, DNA was sonicated using a Qsonica S-4000 with a 1/16" tip for 3 minutes, with 10 second pulses at intensity 3.5, and 20 seconds rest between pulses. DNA was then purified using the MinElute PCR Purificaiton Kit (Qiagen #28006), with elution in a total volume of 300 μL 1× EB buffer.

For streptavidin pulldown of biotin-labeled DNA, 150

μL of 10 mg/mL Dynabeads MyOne Streptavidin T1 beads (Life Technologies, 65602) were separated on a magnetic stand, then washed with 400 μL of 1× TWB (Tween Washing Buffer; 5 mM Tris-HCl pH 7.5; 0.5 mM EDTA; 1 M NaCl; 0.05% Tween 20). The beads were resuspended in 300 μL of 2× Binding Buffer (10 mM Tris-HCl pH 7.5, 1 mM EDTA; 2 M NaCl), the sonicated DNA was added, and the beads were incubated for ≥15 minutes at room temperature on a rotator. After separation on a magnetic stand, the beads were washed with 600 μL of 1× TWB, and heated at 55 °C in a Thermomixer with shaking for 2 minutes. After removal of the supernatant on a magnetic stand, the TWB wash and 55 °C incubation were repeated.

Final libraries were prepared on beads using the NEBNext Ultra II DNA Library Prep Kit (NEB, #E7645) as follows. End repair was carried out by resuspending beads in 50 μL 1× EB buffer, and adding 3 μL NEB Ultra End Repair Enzyme and 7 μL NEB Ultra End Repair Enzyme, followed by incubation at 20 °C for 30 minutes and then at 65 °C for 30 minutes.

Adapters were ligated to DNA fragments by adding 30 μL Blunt Ligation mix, 1 μL Ligation Enhancer and 2.5 μL NEB Adapter, incubating at 20 °C for 20 minutes, adding 3 μL USER enzyme, and incubating at 37 °C for 15 minutes.

Beads were then separated on a magnetic stand, and washed with 600 μL TWB for 2 minutes at 55 °C, 1000 rpm in a Thermomixer. After separation on a magnetic stand, beads were washed in 100 μL 0.1 × TE buffer, then resuspended in 16 μL 0.1 × TE buffer, and heated at 98 °C for 10 minutes.

For PCR, 5 μL of each of the i5 and i7 NEB Next sequencing adapters were added together with 25 μL 2× NEB Ultra PCR Mater Mix. PCR was carried out with a 98 °C incubation for 30 seconds and 12 cycles of 98 °C for 10 seconds, 65 °C for 30 seconds, and 72 °C for 1 minute, followed by incubation at 72 °C for 5 minutes.

Beads were separated on a magnetic stand, and the supernatant was cleaned up using 1× AMPure XP beads.

Libraries were sequenced in a paired-end format on a Illumina NextSeq instrument using NextSeq 500/550 high output kits (either 2×75 or 2×36 cycles).

Hi-C data processing and assembly scaffolding

As an initial step, Hi-C sequencing reads from all libraries were trimmed of adapter sequences, pooled together, and processed against the previously published *B. minutum* assembly (19) using the Juicer pipeline (38) for analyzing Hi-C datasets (version 1.8.9 of Juicer Tools).

The resulting Hi-C matrices were then used as input to the 3D DNA pipeline (20) for automated scaffolding with the following parameters: `--editor-coarse-resolution 5000 --editor-coarse-region 5000 --polisher-input-size 100000 --polisher-coarse-resolution 1000 --polisher-coarse-region 300000 --splitter-input-size 100000 --splitter-coarse-resolution 5000 --splitter-coarse-region 300000 --sort-output --build-gapped-map -r 10 -i 5000`.

Manual correction of obvious assembly and scaffolding errors was then carried out using Juicebox (38).

After finalizing the scaffolding, Hi-C reads were reprocessed against the new assembly using the Juicer pipeline. This was done individually for each library as well as together for the pooled set of reads.

Data was extracted from the final read matrices using the Juicer suite of tools for Hi-C data analysis.

Identification of Hi-C domains

Hi-C matrices were first converted to *cool* format using HiCExplorer (**?**) "hicConvertFormat" with parameters `--inputFormat hic --outputFormat h5` and default resolutions. Subsequent HiCExplorer commands were carried out at 10 kb, 25 kb, and 50 kb resolutions with similar results. Matrices were normalized using "hicNormalize" with parameter `--normalize smallest`, and corrected using "hicCorrectMatrix correct" with parameters `--correctionMethod KR`. Hi-C domains were computationally identified using the "hicFindTADs" from HiCExplorer with parameter `--correctForMultipleTesting fdr`.

RNA-seq datasets

Approximately 5×10^7 cells were collected by centrifugation at 100 *g* for 5 minutes at room temperature. Total RNA was extracted and libraries were constructed for RNA-Seq using the TruSeq RNA Library Prep Kit V2 (Illumina, San Diego, CA, USA) according to the manufacturer protocol. All of the raw sequencing reads are available at Sequence Read Archive (SRA) with accession number SRX7258938.

RNA-seq data analysis

RNA-seq reads were aligned against the corresponding assemblies using the STAR aligner (39) (version 2.5.3a) with the following settings: `--limitSjdbInsertNsj 10000000 --outFilterMultimapNmax 50 \verb–outFilterMismatchNmax— 999 --outFilterMismatchNoverReadLmax 0.04 --alignIntronMin 10 --alignIntronMax 1000000 --alignMatesGapMax 1000000 --alignSJoverhangMin 8 --alignSJDBoverhangMin 1 --sjdbScore 1 --twopassMode Basic --twopass1readsN -1`. As available RNA-seq datasets for *B. minutum* are not strand-specific, the strand orientation of the transcriptome was visualized as follows. Aligned reads were first *de novo* assembled into transcripts and quantified at the transcript level using Stringtie (40) (version 1.3.3.b); the orientation of splice junctions serves as a reliable guide for the directionality of these transcripts. Open reading frames (ORFs) were identified for each transcript, and transcripts with ORFs shorter than 60 amino acids were filtered out of the transcript

set. Strand-specific genomic tracks were then generated by assigning to each basepair covered by at least one exon in that set the sum of the TPM (Transcript Per Million transcripts) values of all transcripts it is included in.

External Hi-C datasets

Hi-C data for *Trypanosoma brucei* was obtained from GEO accession GSE118764.

Hi-C data for *Schizosaccharomyces pombe* was obtained from GEO accession GSE57316.

Hi-C data for *Caulobacter vibrioides* CB15 was obtained from GEO accession GSE45966.

Sequence Analysis

Topoisomerase and other replication-related proteins were identified in annotated MMETSP transcriptome assemblies using HMMER3.0 (41) and the Pfam 27.0 protein domain database (42) as previously described (15).

Supplementary Tables

Supplementary Table 1: Summary of Hi-C datasets used in this study

Hi-C library	Number raw read pairs	Estimated library complexity	Number Hi-C contacts
L142-SSBO1-HIC	534,609,924	920,112,029	220,908,462
L533-SSBO1_27C_Hi-C	556,089,015	1,513,268,498	151,618,419
L534-SSBO1_34C_Hi-C	531,461,453	2,971,291,849	165,231,965
L1240-SSBO1-α_amanitin-0h-Hi-C	111,333,226	233,525,989	34,384,671
L1241-SSB01-α_amanitin-16h-Hi-C-rep1	60,696,609	317,650,525	24,238,281
L1242-SSB01-α_amanitin-16h-Hi-C-rep2	67,376,168	227,736,960	25,551,603
L1243-SSB01-α_amanitin-24h-Hi-C-rep1	81,532,584	235,898,386	29,748,439
L1244-SSB01-α_amanitin-24h-Hi-C-rep2	106,381,220	110,607,925	28,845,306
L1245-SSB01-α_amanitin-48h-Hi-C-rep1	90,180,763	155,046,434	27,045,343
L1246-SSB01-α_amanitin-48h-Hi-C-rep2	78,982,528	152,703,652	22,153,117
L1247-SSB01-α_amanitin_high-48h-Hi-C	110,015,013	157,350,902	28,138,017
L1332-SSB01-α_amanitin-0h-Hi-C-technical_rep	117,543,007	182,213,300	34,089,285
L1333-SSB01-α_amanitin-48h-Hi-C-rep1-technical_rep	117,821,773	82,740,021	23,654,760
L1334-SSB01-α_amanitin_high-48h-Hi-C-technical_rep	95,662,202	164,149,035	23,944,231
L1336-SSB01-α_amanitin_high-24h-Hi-C-second_time_course	58,747,402	103,174,104	15,663,160
L1337-SSB01-α_amanitin_high-48h-Hi-C-second_time_course	83,691,617	62,658,394	14,523,464
L1344-SSB01-α_amanitin/triptolide_0h_NT-Hi-C	79,383,186	208,157,102	23,592,335
L1346-SSB01-triptolide_8h_normal_dose-Hi-C	81,731,190	193,514,340	22,700,096
L1347-SSB01-triptolide_8h_high_dose-Hi-C	112,753,865	187,235,670	28,552,855
L1348-SSB01-Triptolide_24h NT-Hi-C	52,148,987	166,057,825	15,674,551
L1349-SSB01-triptolide_24h_normal_dose-Hi-C	132,715,807	206,778,720	36,745,591
L1350-SSB01-triptolide_24h_high_dose-Hi-C	98,429,444	265,027,975	32,121,298
L1351-SSB01-Triptolide_48h NT-Hi-C	96,846,551	240,797,245	28,296,251
L1352-SSB01-triptolide_48h_normal_dose-Hi-C	85,347,611	255,500,603	25,051,605
L1353-SSB01-triptolide_48h_high_dose-Hi-C	99,978,207	215,504,692	26,572,806

Supplementary Table 2: Inventory of topoisomerases and some other proteins involved in DNA replication in dinoflagellates and other eukaryotes as annotated by transcriptome assemblies in the MMETSP databses

clade	species	TOP1	TOP2	TOP3	MCM	PCNA	RPA1	RPA2	RPA3	RFC1
Amoebozoa	*Stereomyxa ramosa* Chinc5	1	2	2	6	2	3	0	2	1
Amoebozoa	*Vexillifera* sp. DIVA3 564 2	1	2	2	7	1	2	0	0	1
Apicomplexa	*Lankesteria abbottii* Grappler Inlet BC	1	1	0	12	5	1	0	0	1
Bicosoecid	Bicosoecid sp ms1	1	0	0	3	1	1	1	1	0
Bicosoecid	*Cafeteria roenbergensis* E4 10	1	0	2	6	1	0	0	1	0
Bicosoecid	*Cafeteria* sp. Caron Lab Isolate	1	1	4	15	1	1	0	1	1
Bolidophyte	*Bolidomonas pacifica* CCMP 1866	2	5	7	8	1	1	0	0	1
Chlorarachniophyte	*Bigelowiella natans* CCMP1258.1	1	1	9	3	1	4	1	0	0
Chlorarachniophyte	*Bigelowiella natans* CCMP1259	1	1	6	7	1	4	1	0	1
Chlorarachniophyte	*Bigelowiella natans* CCMP 2755	0	0	4	5	1	4	1	0	1
Chlorarachniophyte	*Bigelowiella natans* CCMP623	1	3	7	9	1	2	1	0	1
Chlorarachniophyte	*Chlorarachnion reptans* CCCM449	2	4	8	11	2	3	1	0	1
Chlorarachniophyte	*Lotharella amoebiformis* CCMP2058	2	6	5	10	1	4	1	0	1
Chlorarachniophyte	*Lotharella globosa* CCCM811	1	2	1	0	1	1	1	1	1
Chlorarachniophyte	*Lotharella oceanica* CCMP622	1	0	0	1	1	2	1	1	1
Chlorarachniophyte	*Norrisiella sphaerica* BC52	1	0	3	0	1	2	1	1	0
Chlorarachniophyte	*Partenskyella glossopodia* RCC365	1	2	1	7	1	3	1	2	1
Chlorophyte	*Bathycoccus prasinos* CCMP1898	1	2	3	9	1	2	0	0	0
Chlorophyte	*Bathycoccus prasinos* RCC716	1	2	3	7	1	3	0	0	1
Chlorophyte	*Chlamydomonas* cf sp CCMP681	1	0	0	5	2	1	0	0	1
Chlorophyte	*Crustomastix stigmata* CCMP3273	1	2	4	10	1	1	1	0	1
Chlorophyte	*Cyanoptyche gloeocystis* SAG4.97	1	0	0	4	1	1	1	0	0
Chlorophyte	*Dolichomastix tenuilepis* CCMP3274	1	1	3	1	2	1	0	1	1
Chlorophyte	*Dunaliella tertiolecta* CCMP1320	1	2	3	10	1	2	0	1	1
Chlorophyte	*Mantoniella antarctica* SL 175	1	8	4	13	1	2	2	1	1
Chlorophyte	*Mantoniella* sp CCMP1436	1	2	1	2	1	1	1	1	1
Chlorophyte	*Micromonas* sp CCMP2099	1	2	2	9	1	2	0	1	1
Chlorophyte	*Micromonas* sp NEPCC29	1	2	3	7	1	2	0	1	1
Chlorophyte	*Micromonas* sp RCC472	1	2	2	7	1	2	1	0	1
Chlorophyte	*Nephroselmis pyriformis* CCMP717	1	4	8	10	1	2	0	1	1
Chlorophyte	*Picochlorum oklahomensis* CCMP2329	1	2	2	6	2	2	1	0	1
Chlorophyte	*Picochlorum* sp. RCC944	1	1	2	6	1	2	0	2	1
Chlorophyte	*Picocystis salinarum* CCMP1897	1	2	1	8	2	2	1	2	1
Chlorophyte	*Polytomella parva* SAG 63 3	1	5	3	18	2	3	0	0	1
Chlorophyte	*Prasinoderma coloniale* CCMP1413	1	2	0	2	1	1	0	0	0
Chlorophyte	*Prasinoderma singularis* RCC927	1	1	1	7	1	1	0	1	1
Chlorophyte	*Pterosperma* sp. CCMP1384	1	0	0	3	1	1	1	1	1
Chlorophyte	*Pycnococcus provasolii* RCC2336	1	1	0	9	1	1	0	0	1
Chlorophyte	*Pycnococcus provasolii* RCC931	1	0	0	7	1	1	0	0	1
Chlorophyte	*Pyramimonas parkeae* CCMP726	1	0	4	7	1	2	1	1	1
Chlorophyte	*Stichococcus* sp RCC1054	1	1	1	8	1	1	0	0	1
Chlorophyte	*Tetraselmis chuii* PLY429	2	0	0	0	0	2	0	1	2
Chlorophyte	*Tetraselmis striata* LANL1001	1	4	4	11	1	2	0	1	1
Choanoflagellata	*Acanthoeca* like sp 10tr	1	3	4	10	1	1	0	1	1
Chromerida	*Chromera velia* CCMP2878	1	1	3	10	2	2	0	0	1
Chromerida	*Vitrella brassicaformis* CCMP3346	1	1	2	9	2	1	0	0	1
Chrysophyte	*Chromulina nebulosa* UTEXLB2642	1	1	1	2	1	1	0	0	1
Chrysophyte	*Dinobryon* sp UTEXLB2267	1	3	0	8	1	1	0	0	1
Chrysophyte	*Mallomonas* Sp CCMP3275	1	2	1	9	1	1	0	1	1
Chrysophyte	*Ochromonas* sp CCMP1393	1	2	2	7	1	1	0	0	1
Chrysophyte	*Paraphysomonas bandaiensis* Caron Lab Isolate	1	2	3	9	2	1	1	1	1
Chrysophyte	*Paraphysomonas imperforata* PA2	0	1	3	6	1	1	1	1	1
Chrysophyte	*Pelagococcus subviridis* CCMP1429	1	1	2	11	1	0	0	0	1
Chrysophyte	*Spumella elongata* CCAP 955 1	1	1	3	10	4	3	0	1	1
Ciliate	*Aristerostoma* sp. ATCC 50986	2	1	1	0	2	1	0	0	2
Ciliate	*Blepharisma japonicum* Stock R1072	0	0	0	7	4	1	0	0	0

Continued on next page

Supplementary Table 2 – *Continued from previous page*

clade	species	TOP1	TOP2	TOP3	MCM	PCNA	RPA1	RPA2	RPA3	RFC1
Ciliate	*Climacostomum virens* Stock W 24	1	2	2	9	3	1	0	0	3
Ciliate	*Condylostoma magnum* COL2	0	0	0	2	0	0	0	0	0
Ciliate	*Euplotes focardii* TN1	1	0	0	5	2	1	0	2	0
Ciliate	*Euplotes harpa* FSP1.4	2	0	5	3	1	0	0	1	0
Ciliate	*Fabrea salina* Unknown	1	1	3	7	2	3	0	0	2
Ciliate	*Favella taraikaensis* FeNarragansettBay	0	1	2	7	3	0	0	0	0
Ciliate	*Litonotus pictus* P1	1	1	2	0	0	0	0	0	0
Ciliate	*Mesodinium pulex* SPMC105	2	13	2	16	9	4	0	0	6
Ciliate	*Myrionecta rubra* CCMP2563	0	1	4	11	1	1	0	1	0
Ciliate	*Platyophrya macrostoma* WH	4	4	4	23	4	6	0	0	3
Ciliate	*Protocruzia adherens* Boccale	3	1	0	9	3	3	0	0	1
Ciliate	*Pseudokeronopsis* sp. OXSARD2	1	1	1	6	1	0	0	1	1
Ciliate	*Strombidinopsis acuminatum* SPMC142	2	6	0	32	10	5	0	0	0
Ciliate	*Strombidinopsis* sp. SopsisLIS2011	1	0	0	8	3	2	0	0	0
Ciliate	*Strombidium* inclinatum S3	1	1	2	8	1	1	0	0	1
Ciliate	*Strombidium rassoulzadegani* ras09	1	0	1	6	1	1	0	1	0
Ciliate	*Tiarina fusus* LIS	1	7	3	16	3	4	2	1	1
Cryptophyte	*Chroomonas mesostigmatica* cf CCMP1168	1	5	4	8	1	2	2	0	1
Cryptophyte	*Cryptomonas curvata* CCAP979 52	2	0	2	0	1	1	0	1	0
Cryptophyte	*Cryptomonas paramecium* CCAP977 2a	3	2	2	5	1	1	0	0	1
Cryptophyte	*Geminigera cryophila* CCMP2564	2	1	5	11	1	2	0	1	2
Cryptophyte	*Geminigera* sp. Caron Lab Isolate	1	3	5	18	1	5	0	1	1
Cryptophyte	*Goniomonas pacifica* CCMP1869	8	4	4	12	1	5	1	3	7
Cryptophyte	*Guillardia theta* CCMP 2712	1	0	2	3	1	1	0	1	0
Cryptophyte	*Hemiselmis andersenii* CCMP644	1	2	5	12	1	2	0	1	1
Cryptophyte	*Hemiselmis rufescens* PCC563	1	0	3	7	1	1	1	1	1
Cryptophyte	*Hemiselmis tepida* CCMP443	3	2	0	3	1	1	1	1	1
Cryptophyte	*Hemiselmis viresens* PCC157	1	0	0	7	1	1	0	1	0
Cryptophyte	*Palpitomonas bilix* NIES 2562	0	1	2	13	4	3	0	1	3
Cryptophyte	*Proteomonas sulcata* CCMP704	0	1	0	3	1	1	0	0	1
Cryptophyte	*Rhodomonas lens* RHODO	2	3	2	2	2	2	0	1	0
Cryptophyte	*Rhodomonas* sp. CCMP768	1	0	1	0	1	1	0	0	0
Diatome	*Amphiprora* sp.	1	4	3	9	1	1	0	0	1
Diatome	*Amphora coffeaeformis* CCMP127	1	1	0	4	1	1	0	0	0
Diatome	*Asterionellopsis glacialis* CCMP134	1	7	1	10	1	1	0	0	1
Diatome	*Astrosyne radiata* 13vi08 1A	1	8	3	6	3	2	0	0	1
Diatome	*Attheya septentrionalis* CCMP2084	1	2	0	9	1	1	0	0	1
Diatome	*Aulacoseira subarctica* CCAP 1002 5	1	2	3	8	2	1	0	0	1
Diatome	*Chaetoceros affinis* CCMP159	1	3	1	8	1	1	0	0	1
Diatome	*Chaetoceros curvisetus*	1	4	4	6	1	3	0	0	1
Diatome	*Chaetoceros debilis* MM31A_1	1	3	1	12	1	1	0	0	1
Diatome	*Chaetoceros neogracile* CCMP1317	1	9	3	10	1	1	0	1	1
Diatome	*Coscinodiscus wailesii* CCMP2513	1	3	6	10	1	1	0	1	1
Diatome	*Craspedostauros australis* CCMP3328	1	0	0	4	0	1	0	0	0
Diatome	*Cyclophora tenuis* ECT3854	1	1	0	3	1	1	0	0	0
Diatome	*Cyclotella meneghiniana* CCMP 338	1	4	3	8	1	1	0	0	1
Diatome	*Cylindrotheca closterium* KMMCC:B 181	3	7	3	14	1	2	0	0	1
Diatome	*Dactyliosolen fragilissimus* Unknown	1	3	3	8	1	1	0	1	1
Diatome	*Ditylum brightwellii* GSO103	1	4	3	11	1	1	0	1	1
Diatome	*Ditylum brightwellii* GSO104	1	4	5	10	1	1	0	1	1
Diatome	*Ditylum brightwellii* GSO105	1	2	3	11	2	1	0	1	1
Diatome	*Entomoneis* sp. CCMP2396	0	1	0	0	1	1	0	0	0
Diatome	*Eucampia antarctica* CCMP1452	1	3	0	5	1	1	1	1	1
Diatome	*Extubocellulus spinifer* CCMP396	1	4	10	13	2	5	3	1	2
Diatome	*Fragilariopsis kerguelensis* L2_C3	1	3	3	11	1	1	2	0	1
Diatome	*Fragilariopsis kerguelensis* L26_C5	1	3	5	22	1	1	3	0	1
Diatome	*Grammatophora oceanica* CCMP 410	1	1	3	5	1	1	0	0	1
Diatome	*Helicotheca tamensis* CCMP826	0	1	0	1	1	1	0	1	0
Diatome	*Leptocylindrus danicus* var. apora B651	3	5	3	0	3	2	0	1	1

Continued on next page

Supplementary Table 2 – *Continued from previous page*

clade	species	TOP1	TOP2	TOP3	MCM	PCNA	RPA1	RPA2	RPA3	RFC1
Diatome	*Leptocylindrus danicus* var. danicus B650	3	11	3	19	1	1	0	1	2
Diatome	*Licmophora paradoxa* CCMP2313	1	1	3	7	1	2	0	0	1
Diatome	*Minutocellus polymorphus* CCMP3303	0	0	0	3	1	1	1	1	0
Diatome	*Minutocellus polymorphus* NH13	2	8	7	21	1	0	1	0	3
Diatome	*Minutocellus polymorphus* RCC2270	1	2	1	7	1	1	1	1	1
Diatome	*Nitzschia punctata* CCMP561	1	2	2	9	1	1	1	1	1
Diatome	*Odontella aurita* isolate 1302 5	1	3	7	11	2	2	1	1	1
Diatome	*Odontella sinensis* Grunow 1884	1	3	0	2	1	1	1	1	1
Diatome	*Proboscia alata* PI_D3	1	7	2	21	1	1	2	0	1
Diatome	*Pseudo-nitzschia australis* 10249_10_AB	1	3	4	8	1	1	1	0	1
Diatome	*Pseudo-nitzschia fradulenta* WWA7	2	11	6	24	4	5	0	0	3
Diatome	*Rhizosolenia setigera* CCMP 1694	1	7	4	18	1	2	0	0	2
Diatome	*Skeletonema dohrnii* SkelB	1	2	0	14	1	1	2	1	1
Diatome	*Skeletonema marinoi* SkelA	1	1	2	7	1	1	2	0	1
Diatome	*Skeletonema menzelii* CCMP793	1	4	4	8	1	1	2	0	1
Diatome	*Stauroneis constricta* CCMP1120	1	0	1	1	1	1	1	0	0
Diatome	*Staurosira complex* sp. CCMP2646	1	3	4	8	1	1	0	1	1
Diatome	*Stephanopyxis turris* CCMP 815	2	0	1	7	3	2	0	1	1
Diatome	*Striatella unipunctata* CCMP2910	4	2	1	6	3	0	1	0	2
Diatome	*Synedropsis recta* cf CCMP1620	1	2	0	1	1	1	1	1	0
Diatome	*Thalassionema frauenfeldii* CCMP 1798	1	5	7	15	1	3	1	1	2
Diatome	*Thalassionema nitzschioides* L26_B	1	3	4	8	1	1	1	1	1
Diatome	*Thalassiosira antarctica* CCMP982	1	4	2	12	1	1	3	1	1
Diatome	*Thalassiosira gravida* GMp14c1	1	1	3	13	1	1	2	1	1
Diatome	*Thalassiosira miniscula* CCMP1093	1	13	6	10	1	1	2	1	1
Diatome	*Thalassiosira oceanica* CCMP1005	1	10	1	10	1	1	0	0	1
Diatome	*Thalassiosira rotula* CCMP3096	1	5	3	11	1	1	2	1	1
Diatome	*Thalassiosira rotula* GSO102	1	3	2	11	1	1	1	1	1
Diatome	*Thalassiosira weissflogii* CCMP1010	1	4	1	9	1	0	1	0	1
Diatome	*Thalassiosira weissflogii* CCMP1336	1	4	1	8	1	0	1	0	1
Diatome	*Thalassiothrix antarctica* L6_D1	1	2	4	6	1	1	0	1	1
Diatome	*Triceratium dubium* CCMP147	0	1	1	1	1	0	1	1	0
Dinoflagellata	*Alexandrium temarense* CCMP1771	3	18	12	45	18	10	3	4	2
Dinoflagellata	*Amphidinium carterae* CCMP1314	2	5	5	8	2	4	0	0	3
Dinoflagellata	*Azadinium spinosum* 3D9	1	12	13	35	11	6	0	0	3
Dinoflagellata	*Brandtodinium nutriculum* RCC3387	1	13	9	30	21	4	0	0	3
Dinoflagellata	*Ceratium fusus* PA161109	1	15	10	18	12	9	1	1	3
Dinoflagellata	*Crypthecodinium cohnii* Seligo	1	6	5	15	2	4	0	0	3
Dinoflagellata	*Dinophysis acuminata* DAEP01	4	15	9	29	13	8	0	0	2
Dinoflagellata	*Durinskia baltica* CSIRO_CS 38	2	12	9	18	9	8	0	0	4
Dinoflagellata	*Gambierdiscus australes* CAWD 149	1	5	0	9	14	6	0	0	2
Dinoflagellata	*Glenodinium foliaceum* CCAP1116_3	2	9	3	23	7	6	0	1	4
Dinoflagellata	*Gonyaulax spinifera* CCMP409	1	2	0	10	10	8	1	1	1
Dinoflagellata	*Heterocapsa rotundata* SCCAP K 0483	2	19	4	12	6	4	0	0	6
Dinoflagellata	*Heterocapsa triquestra* CCMP 448	1	8	5	13	5	4	0	0	3
Dinoflagellata	*Karenia brevis* CCMP2229	1	14	8	10	8	7	0	1	4
Dinoflagellata	*Karenia brevis* SP1	1	14	13	16	6	8	0	1	4
Dinoflagellata	*Karenia brevis* SP3	1	12	9	13	8	10	0	1	4
Dinoflagellata	*Karenia brevis* Wilson	1	14	7	14	9	8	0	2	5
Dinoflagellata	*Karlodinium micrum* CCMP2283	2	9	7	46	13	31	2	0	5
Dinoflagellata	*Kryptoperidinium foliaceum* CCMP1326	4	14	11	64	16	10	1	0	7
Dinoflagellata	*Lingulodinium polyedra* CCMP1738	1	17	8	19	11	11	1	0	3
Dinoflagellata	*Noctiluca scintillans* Unknown	1	7	3	9	1	6	0	1	1
Dinoflagellata	*Oxyrrhis marina*	1	2	5	9	7	3	0	1	2
Dinoflagellata	*Oxyrrhis marina* CCMP1795	0	0	0	0	3	0	0	0	0
Dinoflagellata	*Oxyrrhis marina* LB1974	1	2	4	10	4	2	0	0	2
Dinoflagellata	*Pelagodinium beii* RCC1491	1	8	2	12	11	4	0	0	4
Dinoflagellata	*Peridinium aciculiferum* PAER_2	1	7	5	11	6	5	0	0	3
Dinoflagellata	*Polarella glacialis* CCMP 1383	1	28	5	23	5	5	0	0	8

Continued on next page

Supplementary Table 2 – *Continued from previous page*

clade	species	TOP1	TOP2	TOP3	MCM	PCNA	RPA1	RPA2	RPA3	RFC1
Dinoflagellata	*Prorocentrum minimum* CCMP1329	1	15	6	29	13	6	0	0	3
Dinoflagellata	*Prorocentrum minimum* CCMP2233	1	14	4	29	12	5	0	0	3
Dinoflagellata	*Protoceratium reticulatum* CCCM 535 CCMP 1889	2	20	9	18	11	10	0	0	2
Dinoflagellata	*Pyrodinium bahamense* pbaha01	1	21	8	29	19	11	0	0	3
Dinoflagellata	*Scrippsiella hangoei* like SHHI_4	1	8	6	22	6	16	0	2	2
Dinoflagellata	*Scrippsiella hangoei* SHTV5	1	8	11	14	3	5	0	0	2
Dinoflagellata	*Scrippsiella trochoidea* CCMP3099	1	27	10	38	12	8	1	1	3
Dinoflagellata	*Symbiodinium kawagutii* CCMP2468	0	0	0	0	2	0	0	0	0
Dinoflagellata	*Symbiodinium* sp. C1	1	9	4	9	6	4	0	0	3
Dinoflagellata	*Symbiodinium* sp. C15	1	7	2	12	3	4	1	0	3
Dinoflagellata	*Symbiodinium* sp. CCMP2430	1	7	2	10	7	4	0	0	3
Dinoflagellata	*Symbiodinium* sp. Mp	1	7	3	13	6	3	0	0	3
Dinoflagellata	*Togula jolla* CCCM 725	1	17	3	21	3	6	0	0	4
Discosea	*Mayorella* sp. BSH 02190019	1	3	2	5	1	1	0	1	1
Discosea	*Neoparamoeba aestuarina* SoJaBio B1 5 56 2	3	3	3	12	3	3	0	1	1
Discosea	*Paramoeba atlantica* 621 1 CCAP 1560 9	1	3	2	8	3	2	0	1	1
Discosea	*Pessonella* sp. PRA 29	1	1	3	0	1	5	0	2	3
Discosea	*Stygamoeba regulata* BSH 02190019	3	8	2	7	2	4	0	0	2
Discosea	*Trichosphaerium* sp. Am I 7 wt	2	0	0	1	2	3	0	0	2
Eugelnophyta	*Eutreptiella gymnastica* like CCMP1594	1	1	1	5	2	1	0	1	1
Foraminifera	*Ammonia* sp. Unknown	1	1	3	9	5	2	0	1	1
Foraminifera	*Elphidium margaritaceum* Unknown	1	1	2	8	3	1	1	0	1
Foraminifera	*Rosalina* sp. Unknown	1	0	0	9	5	0	2	0	1
Foraminifera	*Sorites* sp. Unknown	3	3	0	27	12	3	0	0	2
Fungi	*Debaryomyces hansenii* J26	1	0	0	4	0	0	0	0	1
Glaucophyte	*Gloeochaete witrockiana* SAG46_84	2	2	3	9	2	2	1	1	1
Haptophyte	*Calcidiscus leptoporus* RCC1130	1	3	0	7	1	1	1	0	1
Haptophyte	*Chrysochromulina brevifilum* UTEX LB 985	1	2	1	4	1	3	0	1	0
Haptophyte	*Chrysochromulina ericina* CCMP281	2	1	0	10	1	3	1	1	2
Haptophyte	*Chrysochromulina polylepis* CCMP1757	1	3	5	9	1	2	1	1	1
Haptophyte	*Chrysoculter rhomboideus* RCC1486	1	0	0	9	1	0	0	1	0
Haptophyte	*Coccolithus pelagicus* ssp *braarudi* PLY182g	1	3	0	7	1	2	1	1	0
Haptophyte	*Emiliania huxleyi* 374	1	2	1	9	1	1	0	0	0
Haptophyte	*Emiliania huxleyi* 379	1	1	1	0	0	2	0	0	0
Haptophyte	*Emiliania huxleyi* CCMP370	1	3	5	9	0	2	1	1	1
Haptophyte	*Emiliania huxleyi* PLYM219	1	3	4	10	0	2	1	1	1
Haptophyte	*Exanthemachrysis gayraliae* RCC1523	1	2	0	1	1	1	0	1	1
Haptophyte	*Gephyrocapsa oceanica* RCC1303	1	3	5	11	1	1	0	0	1
Haptophyte	*Imantonia* sp. RCC918	3	1	1	4	2	1	1	1	0
Haptophyte	*Isochrysis galbana* CCMP1323	2	5	6	13	2	3	1	0	2
Haptophyte	*Isochrysis* sp. CCMP1244	1	2	5	11	1	1	0	1	1
Haptophyte	*Isochrysis* sp. CCMP1324	1	2	0	12	1	2	1	0	1
Haptophyte	*Pavlova* sp. CCMP459	1	2	1	6	2	1	2	1	1
Haptophyte	*Phaeocystis antarctica* Caron Lab Isolate	3	7	2	12	1	3	2	0	2
Haptophyte	*Phaeocystis* sp. CCMP2710	1	0	1	2	1	1	1	1	1
Haptophyte	*Pleurochrysis carterae* CCMP645	3	2	1	7	1	2	1	1	1
Haptophyte	*Prymnesium parvum* Texoma1	1	6	4	1	1	2	1	1	1
Haptophyte	*Scyphosphaera apsteinii* RCC1455	1	3	1	7	1	2	1	0	1
Heterolobosea	*Percolomonas cosmopolitus* AE 1 ATCC 50343	1	4	2	9	2	2	0	0	1
Heterolobosea	*Percolomonas cosmopolitus* WS	1	3	1	12	1	2	0	0	3
Khakista	*Corethron pennatum* L29A3	2	5	5	16	1	1	1	0	1
Khakista	*Detonula confervacea* CCMP 353	1	3	2	9	1	1	2	1	1
Kinetoplastida	*Neobodo designis* CCAP 1951 1	1	1	4	8	1	1	0	0	1
Labyrinthulida	*Aplanochytrium* sp. PBS07	1	2	1	3	1	1	1	2	1
Labyrinthulida	*Aplanochytrium stocchinoi* GSBS06	1	2	0	7	1	1	1	1	1
Pelagophyte	*Aureococcus anophagefferens* CCMP1850	6	2	3	45	1	2	0	0	1
Pelagophyte	*Aureoumbra lagunensis* CCMP1510	1	2	2	9	1	2	1	0	1
Pelagophyte	*Chrysocystis fragilis* CCMP3189	2	0	2	6	1	1	1	0	1

Continued on next page

Supplementary Table 2 – *Continued from previous page*

clade	species	TOP1	TOP2	TOP3	MCM	PCNA	RPA1	RPA2	RPA3	RFC1
Pelagophyte	*Chrysoreinhardia* sp. CCMP2950	1	2	1	5	0	1	0	0	1
Pelagophyte	*Chrysoreinhardia* sp. CCMP3193	1	3	2	10	1	2	1	0	1
Pelagophyte	*Pelagomonas calceolata* CCMP1756	1	2	1	9	1	1	2	0	1
Pelagophyte	*Sarcinochrysis* sp. CCMP770	0	0	0	2	1	1	1	1	0
Perkinsid	*Perkinsus chesapeaki* ATCC_PRA_65	2	0	0	0	0	0	0	0	0
Perkinsid	*Perkinsus marinus* ATCC50439	1	0	0	1	2	0	0	0	0
Pinguiophyte	*Phaeomonas parva* CCMP2877	1	3	1	5	3	1	0	1	0
Pinguiophyte	*Pinguiococcus pyrenoidosus* CCMP2078	1	2	3	0	1	1	0	1	0
Raphidophyte	*Chattonella subsalsa* CCMP2191	1	3	0	5	1	1	1	0	1
Raphidophyte	*Fibrocapsa japonica* CCMP1661	0	1	1	5	1	1	0	1	0
Raphidophyte	*Heterosigma akashiwo* CCMP2393	1	4	2	11	2	1	0	1	1
Raphidophyte	*Heterosigma akashiwo* CCMP3107	1	7	2	0	1	1	0	0	0
Raphidophyte	*Heterosigma akashiwo* CCMP452	0	1	0	4	1	1	0	0	0
Raphidophyte	*Heterosigma akashiwo* NB	1	6	1	8	1	1	0	1	1
Rhodophyte	*Compsopogon coeruleus* SAG 36.94	1	3	2	11	1	1	0	0	1
Rhodophyte	*Erythrolobus australicus* CCMP3124	1	2	3	0	1	1	0	1	1
Rhodophyte	*Erythrolobus madagascarensis* CCMP3276	1	1	1	3	1	2	0	1	0
Rhodophyte	*Madagascaria erythrocladiodes* CCMP3234	3	4	5	12	1	2	0	1	2
Rhodophyte	*Porphyridium aerugineum* SAG 1380 2	2	1	2	5	1	2	1	0	1
Rhodophyte	*Rhodella maculata* CCMP736	1	3	3	12	1	1	0	0	1
Rhodophyte	*Rhodosorus marinus* CCMP 769	1	8	6	17	0	3	0	0	2
Rhodophyte	*Timspurckia oligopyrenoides* CCMP3278	1	2	4	6	1	2	1	1	1
Silicoflagellates	*Dictyocha speculum* CCMP1381	1	4	2	9	1	2	1	1	1
Silicoflagellates	*Pseudopedinella elastica* CCMP716	1	5	6	9	1	1	1	1	1
Silicoflagellates	*Pteridomonas danica* PT	1	1	1	2	1	1	1	1	0
Silicoflagellates	*Rhizochromulina marina* cf CCMP1243	1	5	2	8	2	2	1	1	1
Synchromophyceae	*Synchroma pusillum* CCMP3072	1	0	1	3	3	1	0	1	1
Syndinian	*Amoebophrya* sp. Ameob2	2	8	1	13	0	1	0	0	0
Thraustochytrid	*Aurantiochytrium limacinum* ATCCMYA1381	1	3	2	9	1	1	0	1	1
Thraustochytrid	*Schizochytrium aggregatum* ATCC28209	1	1	1	4	1	1	0	0	1
Thraustochytrid	*Thraustochytrium* sp. LLF1b	1	2	1	9	1	1	0	1	1
Tubulinid	*Filamoeba nolandi* NC AS 23 1	2	4	1	13	0	3	1	0	1
Tubulinid	*Sexangularia* sp. ATCC50979	0	6	7	14	2	2	1	0	3
Vanellinid	*Vannella robusta* DIVA3 518 3 11 1 6	1	2	3	6	1	2	1	1	1
Vanellinid	*Vannella* sp. DIVA3 517 6 12	6	6	9	13	1	1	0	1	1
Xantophyte	*Vaucheria litorea* CCMP2940	1	2	0	6	1	1	0	1	1

Supplementary Figures

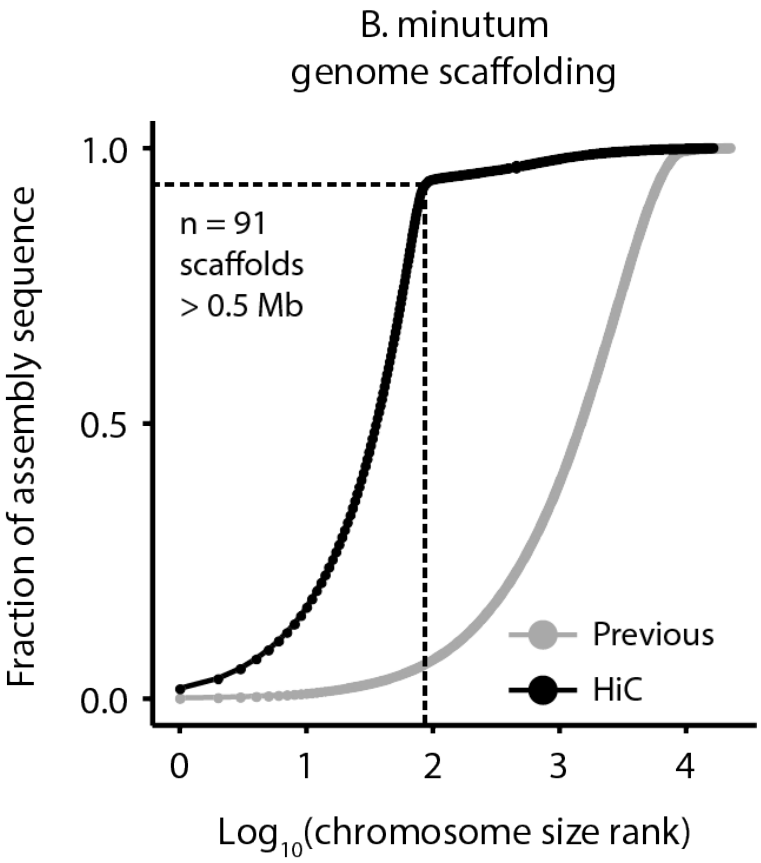

Supplementary Figure 1: Cumulative distribution of scaffolds and pseudochromosome sizes before and after Hi-C scaffolding of the draft *Breviolum/Symbiodinium minutum* assembly (19). 3D DNA(20) scaffolding of the assembly results in 91 major pseudochromosomes ≥500kb encompassing ∼94% of the assembled sequence.

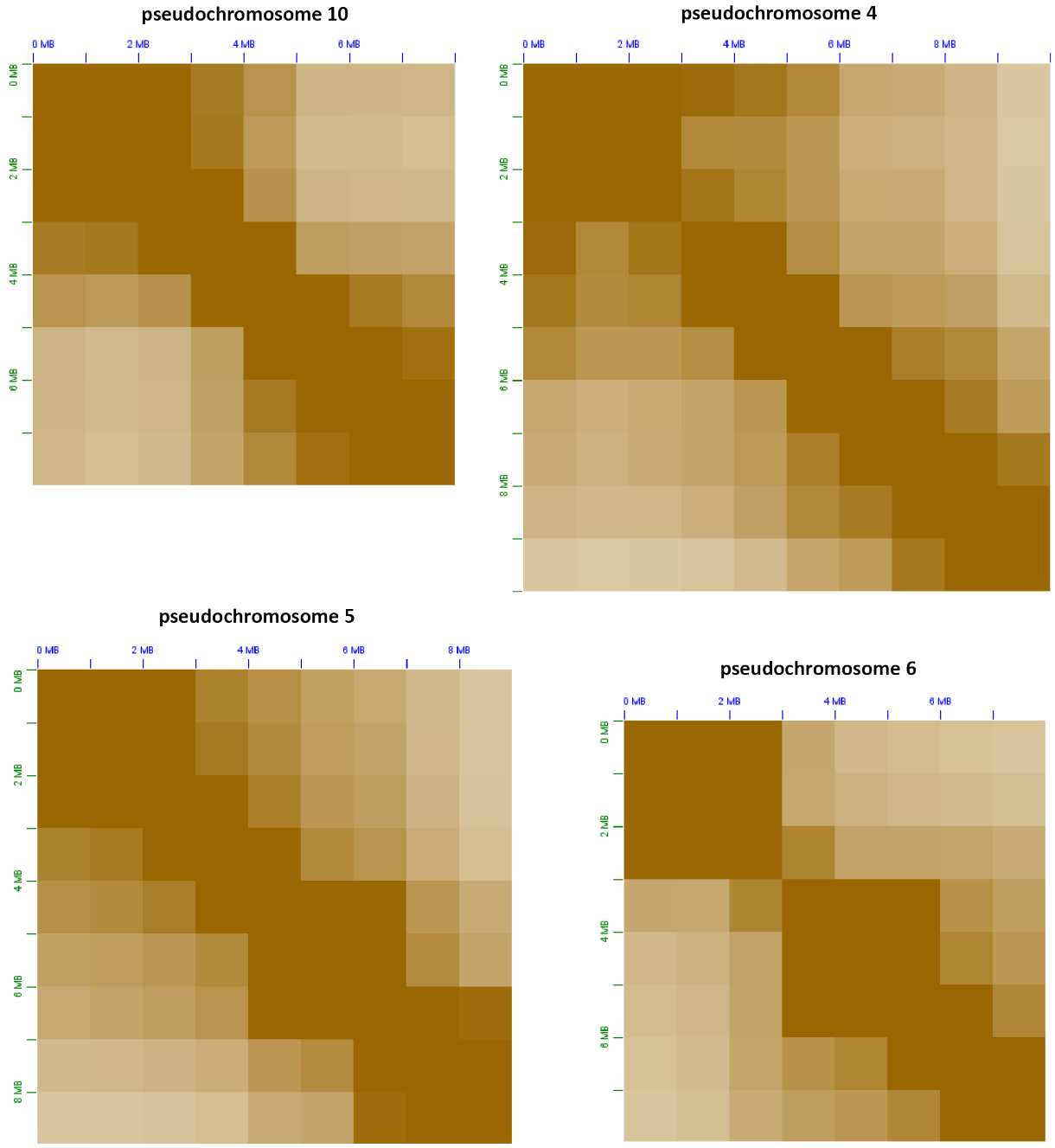

Supplementary Figure 2: Broad-level bipartite to tripartite topological structure of dinoflagellate. Shown are 1Mbp-resolution KR-normalized(1) Hi-C matrices for four of the *B. minutum* pseudochromosomes.

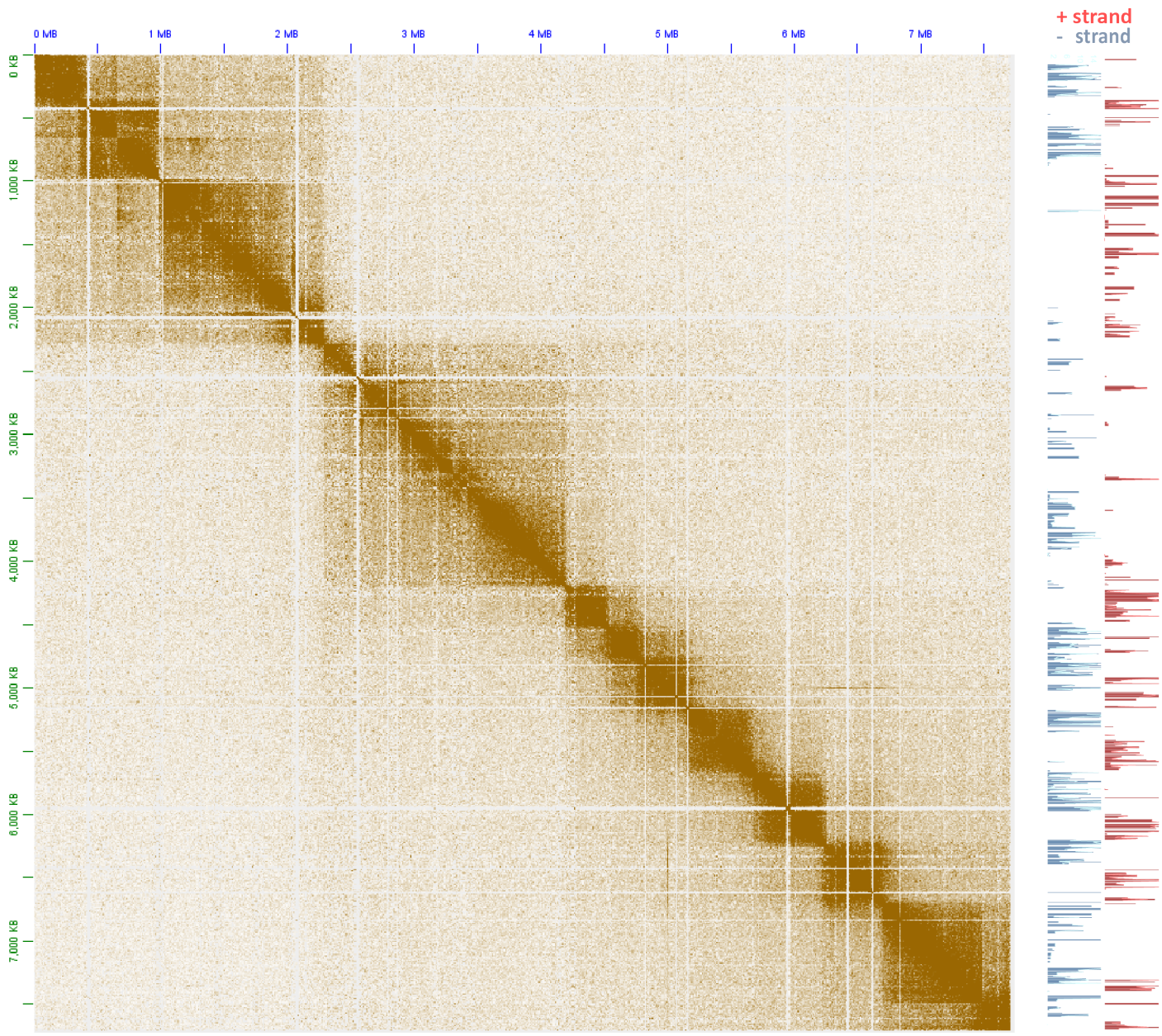

Supplementary Figure 3: The topological domain organization of dinoflagellate chromosomes is related to polycistronic gene array orientation. Shown is the 5kb-resolution KR-normalized Hi-C map together with strand-specific RNA expression levels for pseudochromosome 17.

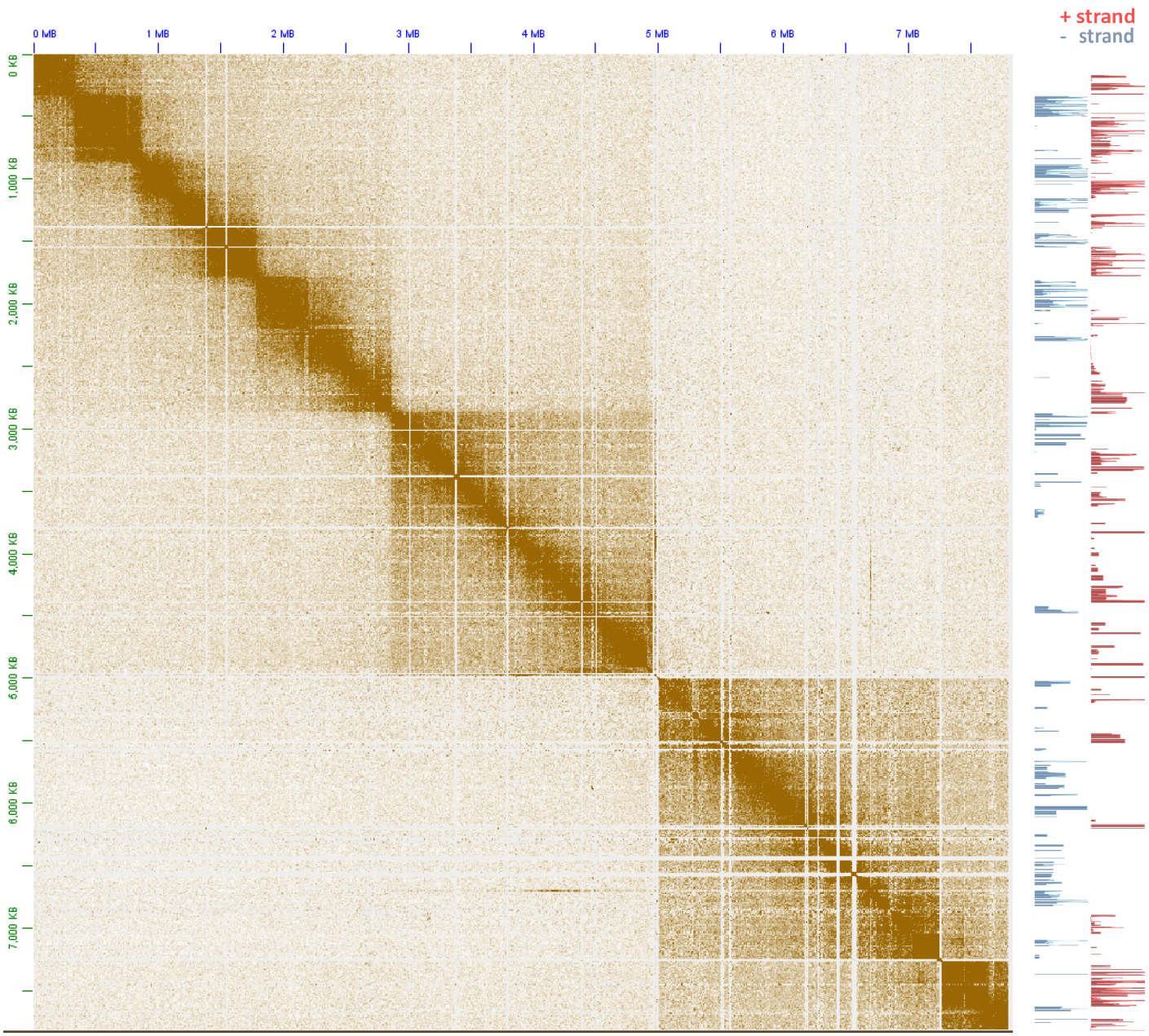

Supplementary Figure 4: The topological domain organization of dinoflagellate chromosomes is related to polycistronic gene array orientation. Shown is the 5kb-resolution KR-normalized Hi-C map together with strand-specific RNA expression levels for pseudochromosome 18.

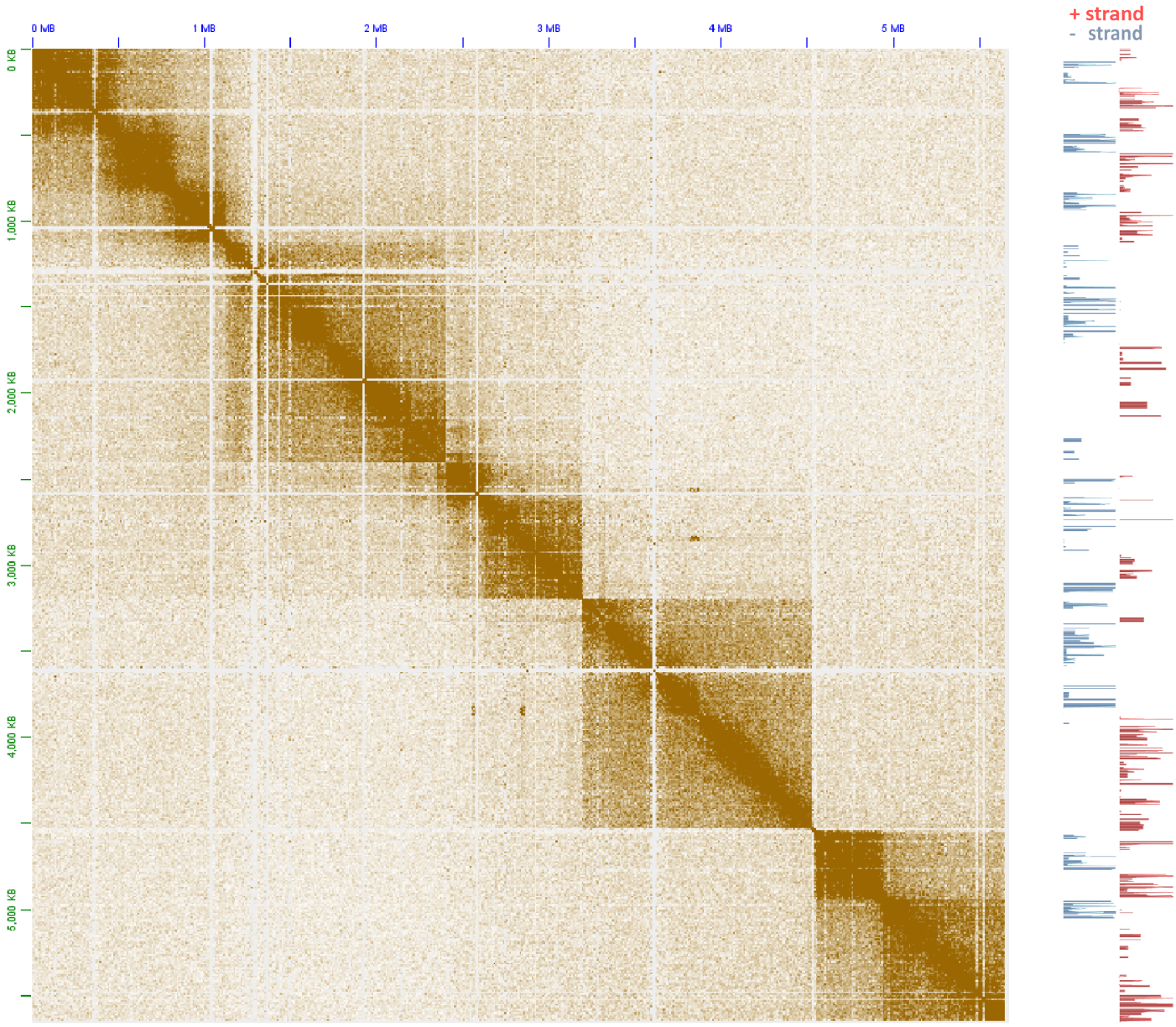

Supplementary Figure 5: The topological domain organization of dinoflagellate chromosomes is related to polycistronic gene array orientation. Shown is the 5kb-resolution KR-normalized Hi-C map together with strand-specific RNA expression levels for pseudochromosome 21.

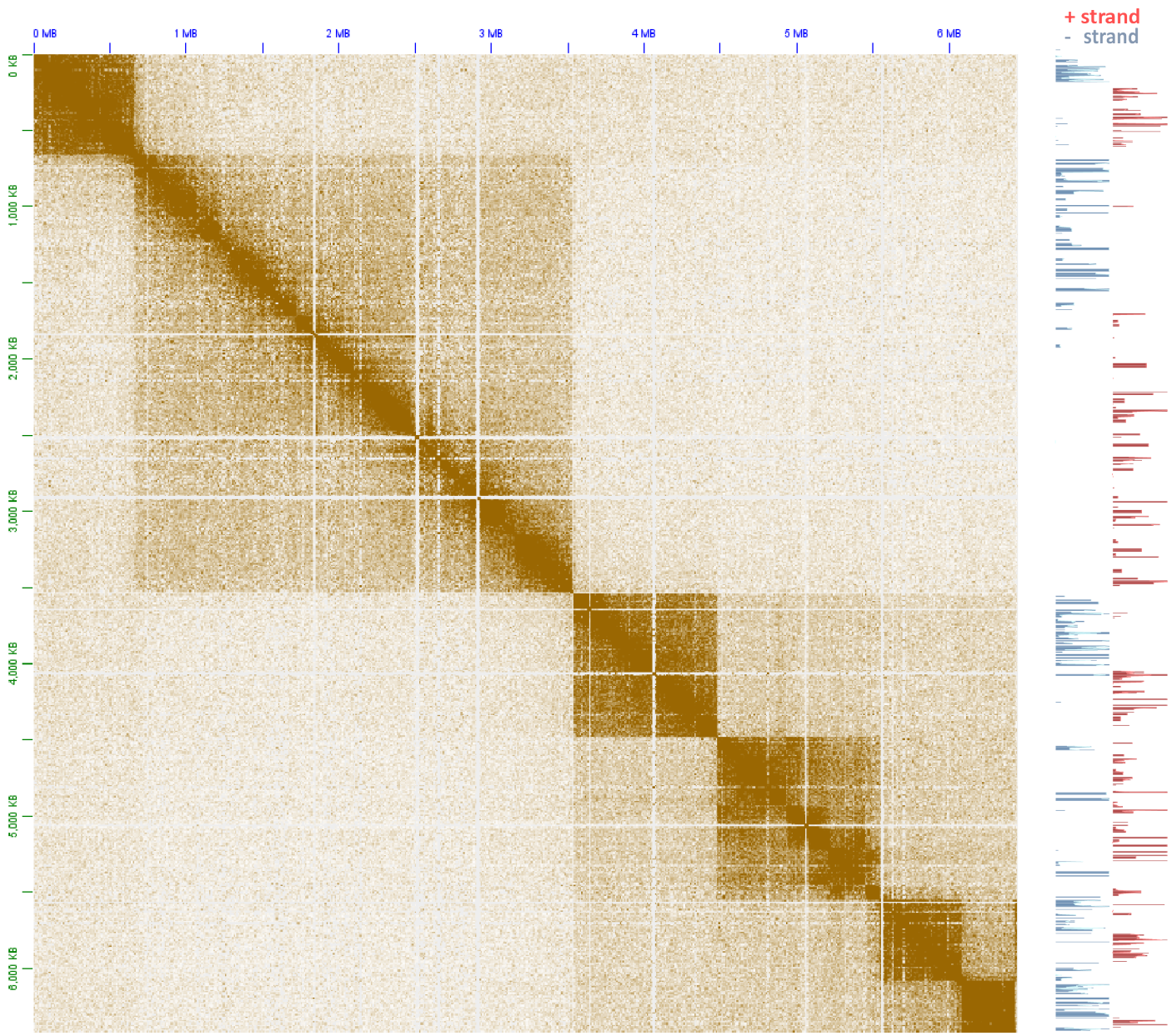

Supplementary Figure 6: The topological domain organization of dinoflagellate chromosomes is related to polycistronic gene array orientation. Shown is the 5kb-resolution KR-normalized Hi-C map together with strand-specific RNA expression levels for pseudochromosome 26.

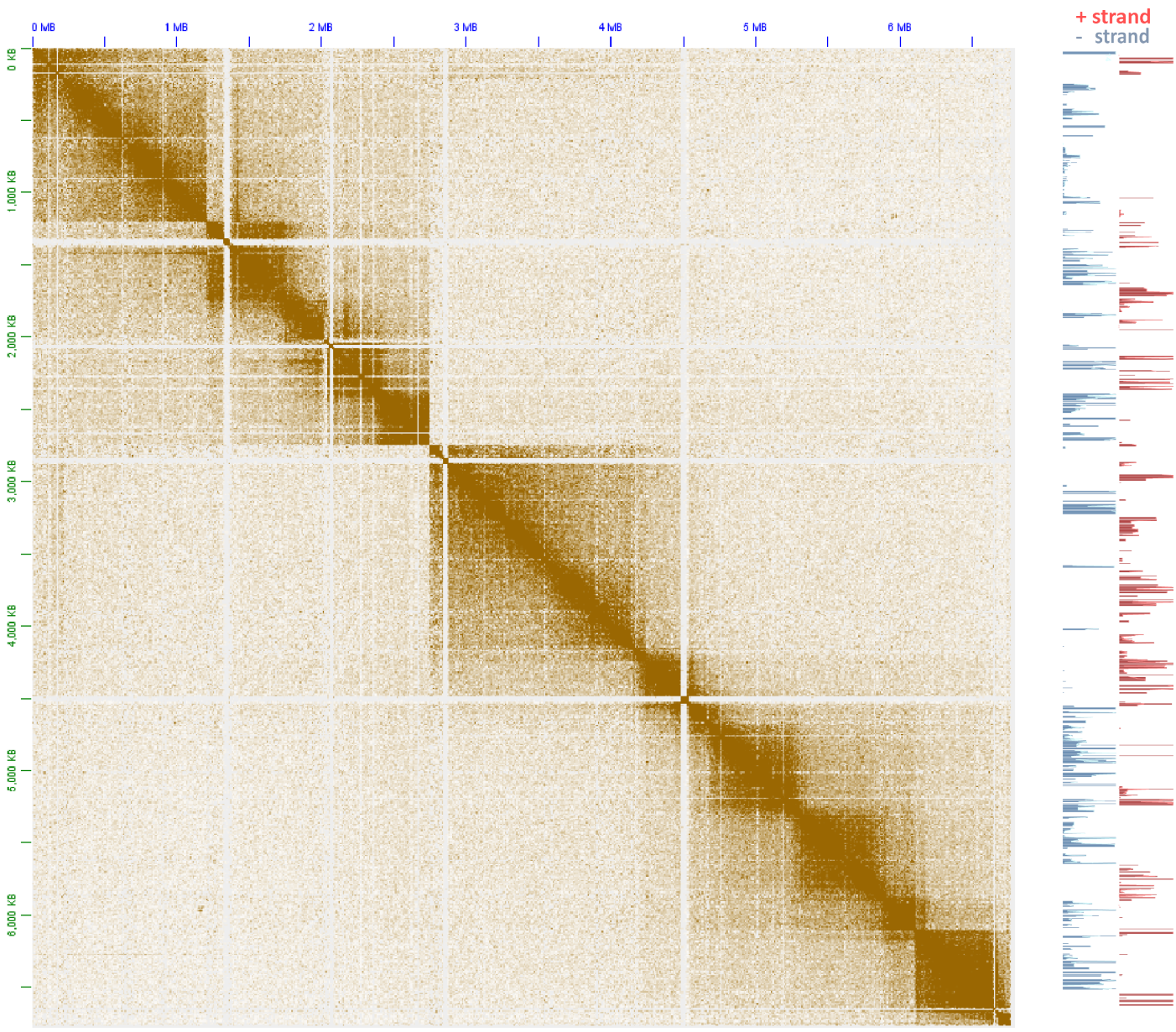

Supplementary Figure 7: The topological domain organization of dinoflagellate chromosomes is related to polycistronic gene array orientation. Shown is the 5kb-resolution KR-normalized Hi-C map together with strand-specific RNA expression levels for pseudochromosome 32.

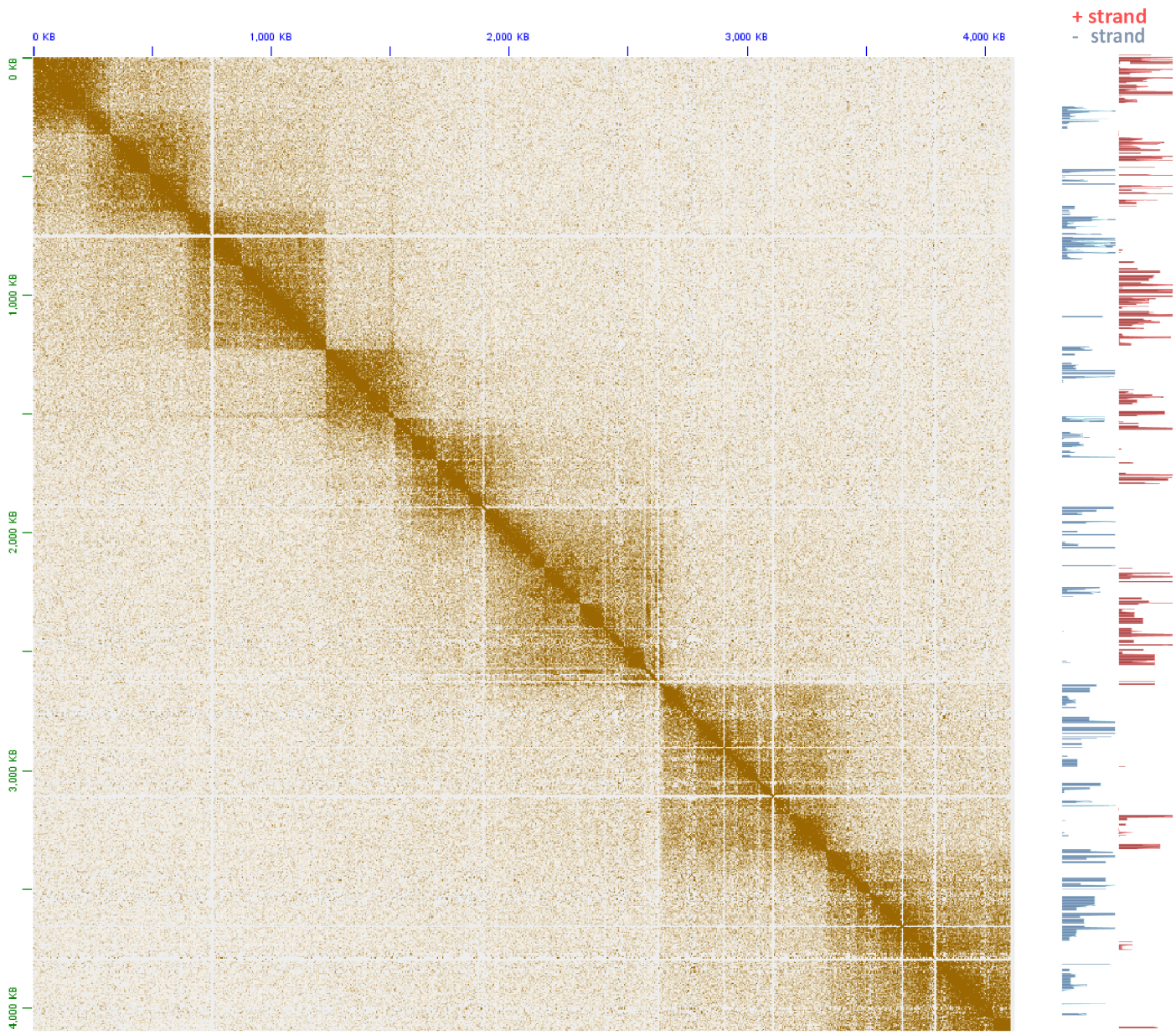

Supplementary Figure 8: The topological domain organization of dinoflagellate chromosomes is related to polycistronic gene array orientation. Shown is the 5kb-resolution KR-normalized Hi-C map together with strand-specific RNA expression levels for pseudochromosome 36.

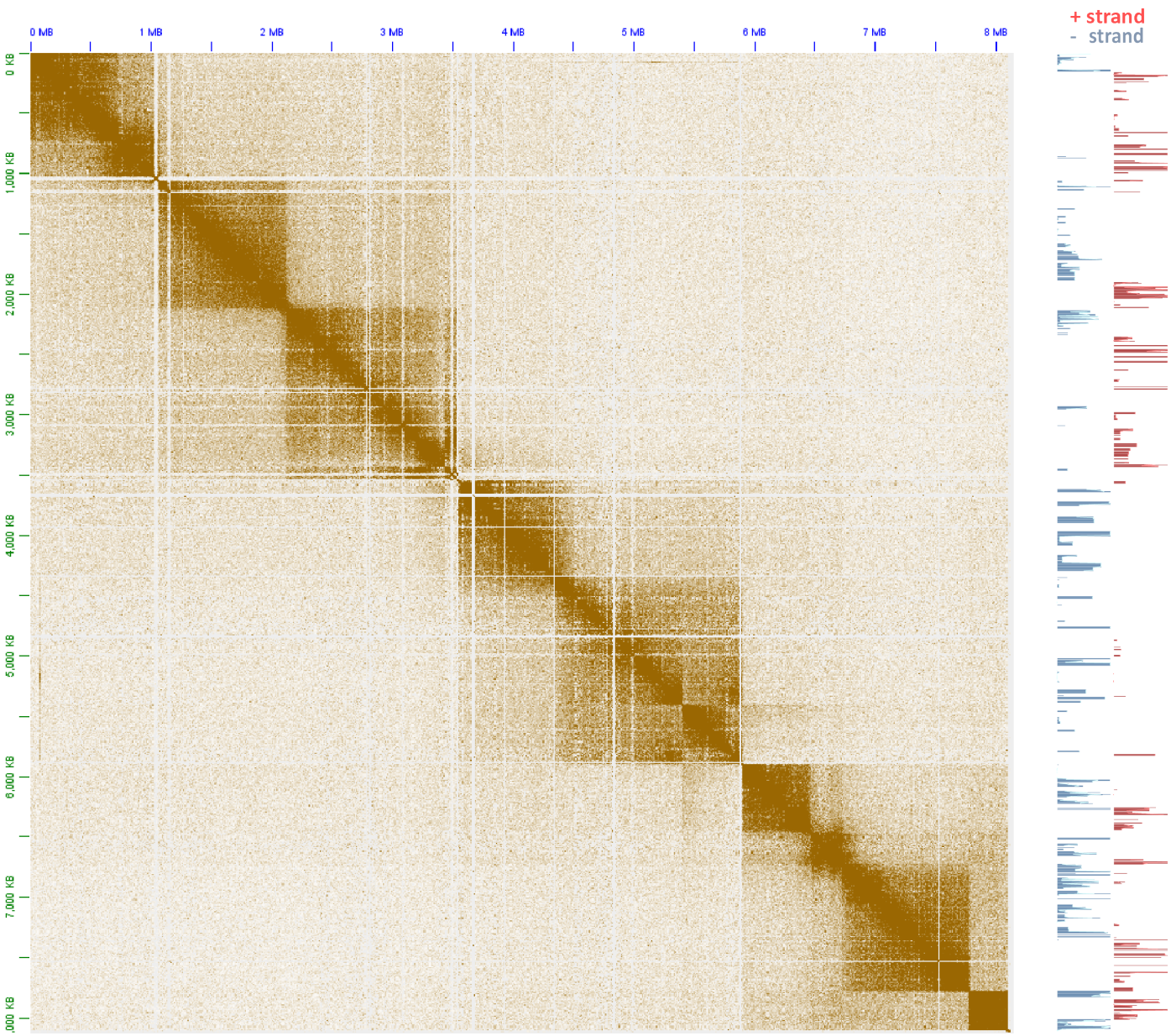

Supplementary Figure 9: The topological domain organization of dinoflagellate chromosomes is related to polycistronic gene array orientation. Shown is the 5kb-resolution KR-normalized Hi-C map together with strand-specific RNA expression levels for pseudochromosome 71.

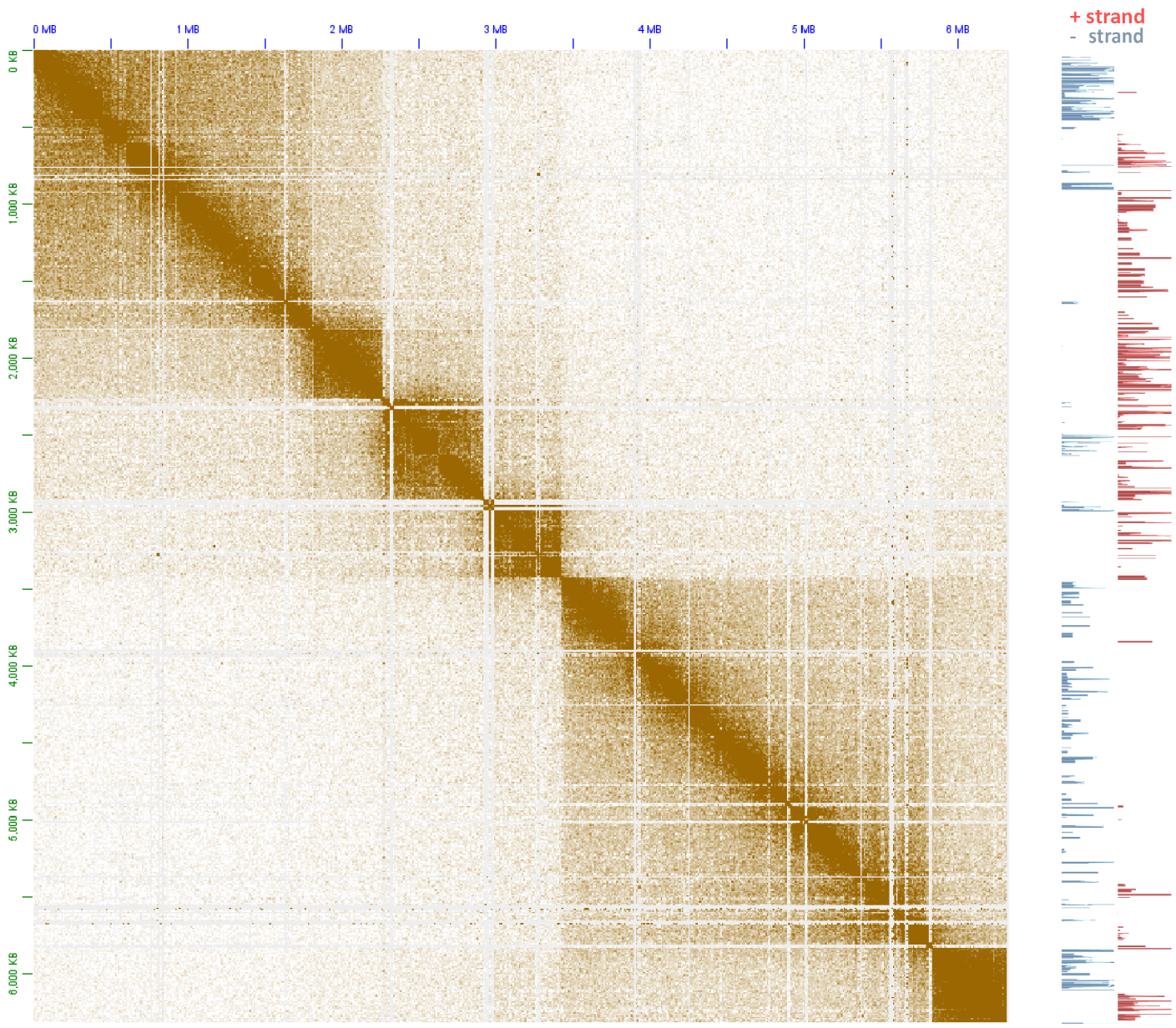

Supplementary Figure 10: The topological domain organization of dinoflagellate chromosomes is related to polycistronic gene array orientation. Shown is the 5kb-resolution KR-normalized Hi-C map together with strand-specific RNA expression levels for pseudochromosome 77.

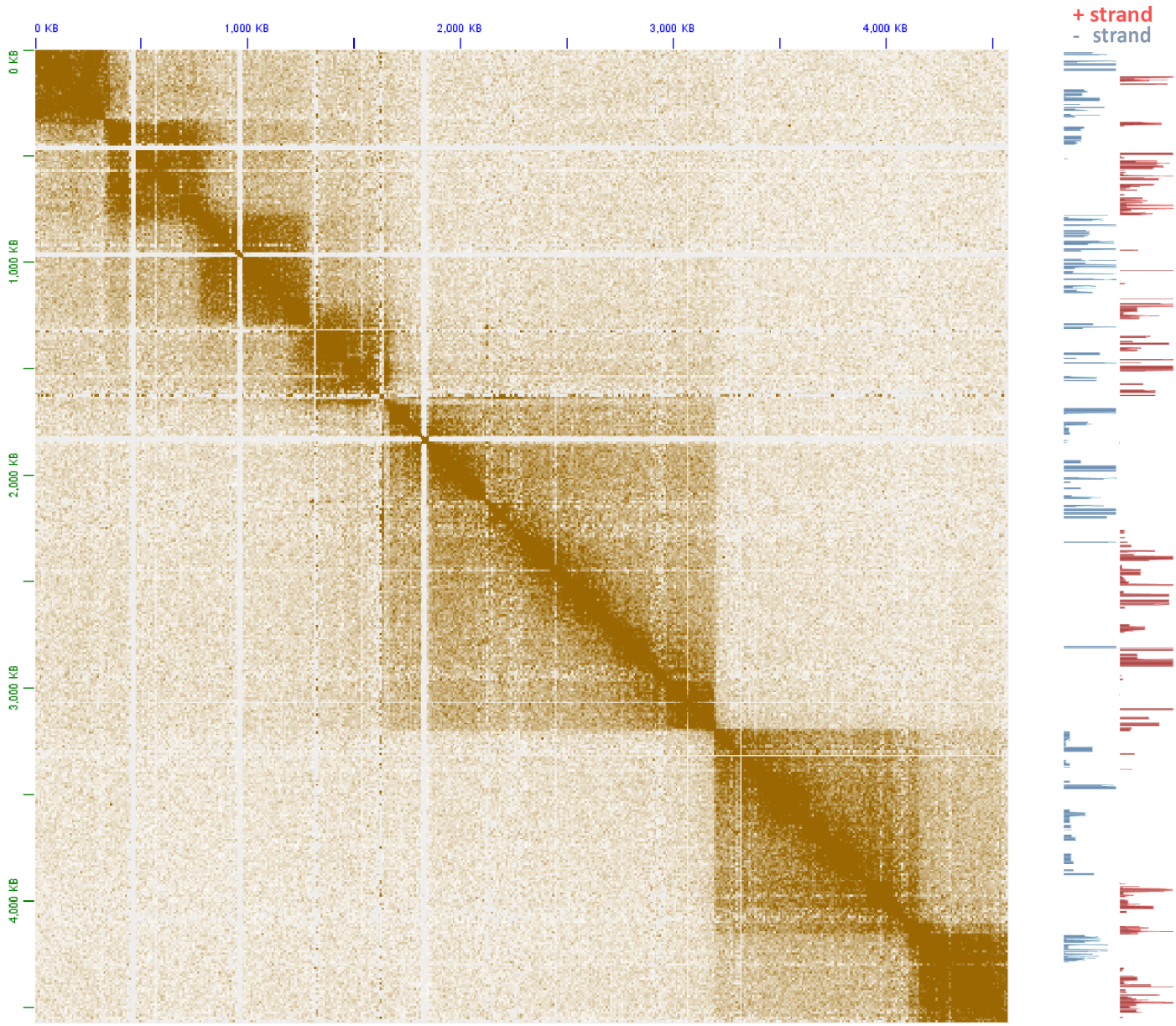

Supplementary Figure 11: The topological domain organization of dinoflagellate chromosomes is related to polycistronic gene array orientation. Shown is the 5kb-resolution KR-normalized Hi-C map together with strand-specific RNA expression levels for pseudochromosome 78.

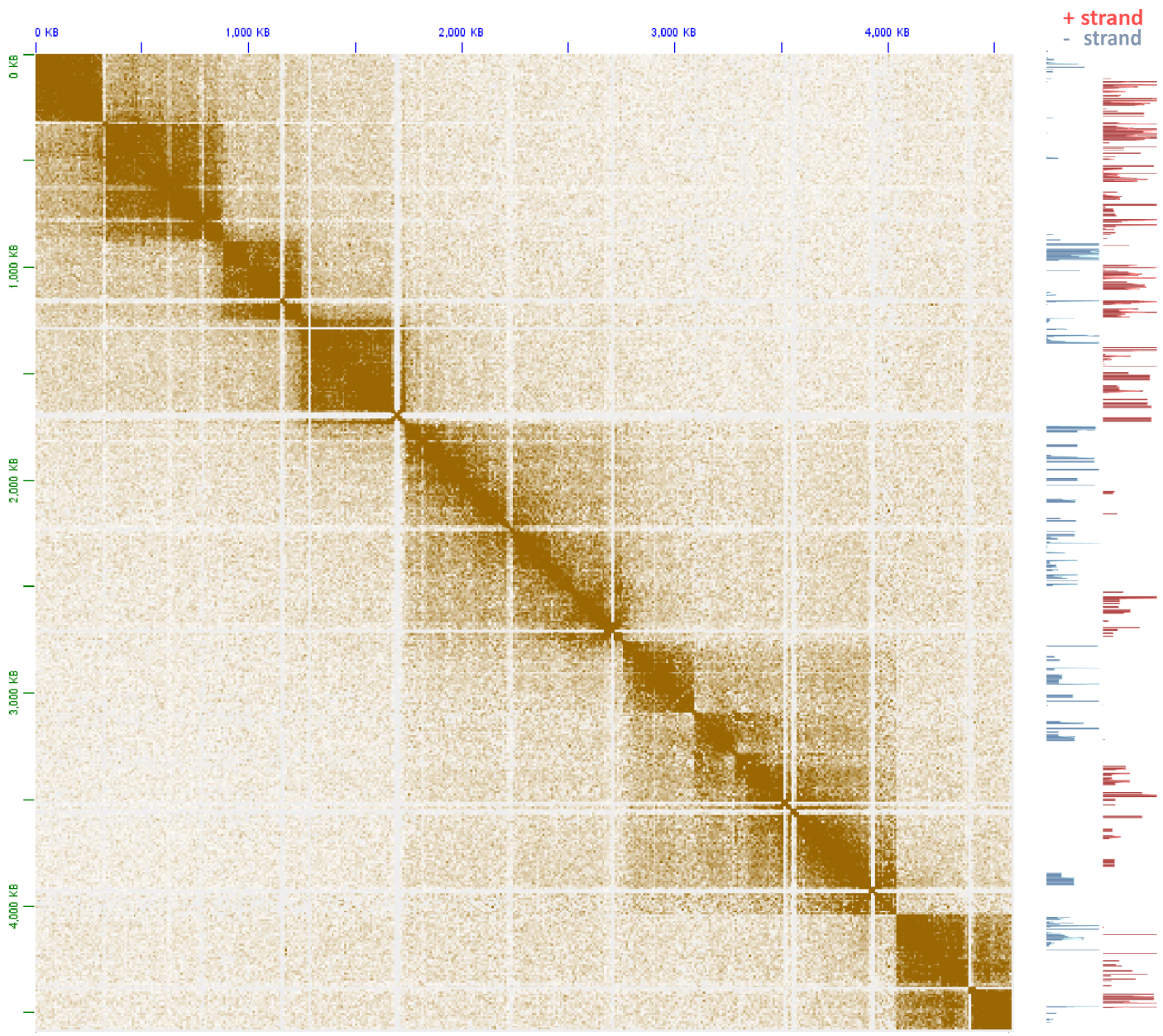

Supplementary Figure 12: The topological domain organization of dinoflagellate chromosomes is related to polycistronic gene array orientation. Shown is the 5kb-resolution KR-normalized Hi-C map together with strand-specific RNA expression levels for pseudochromosome 88.

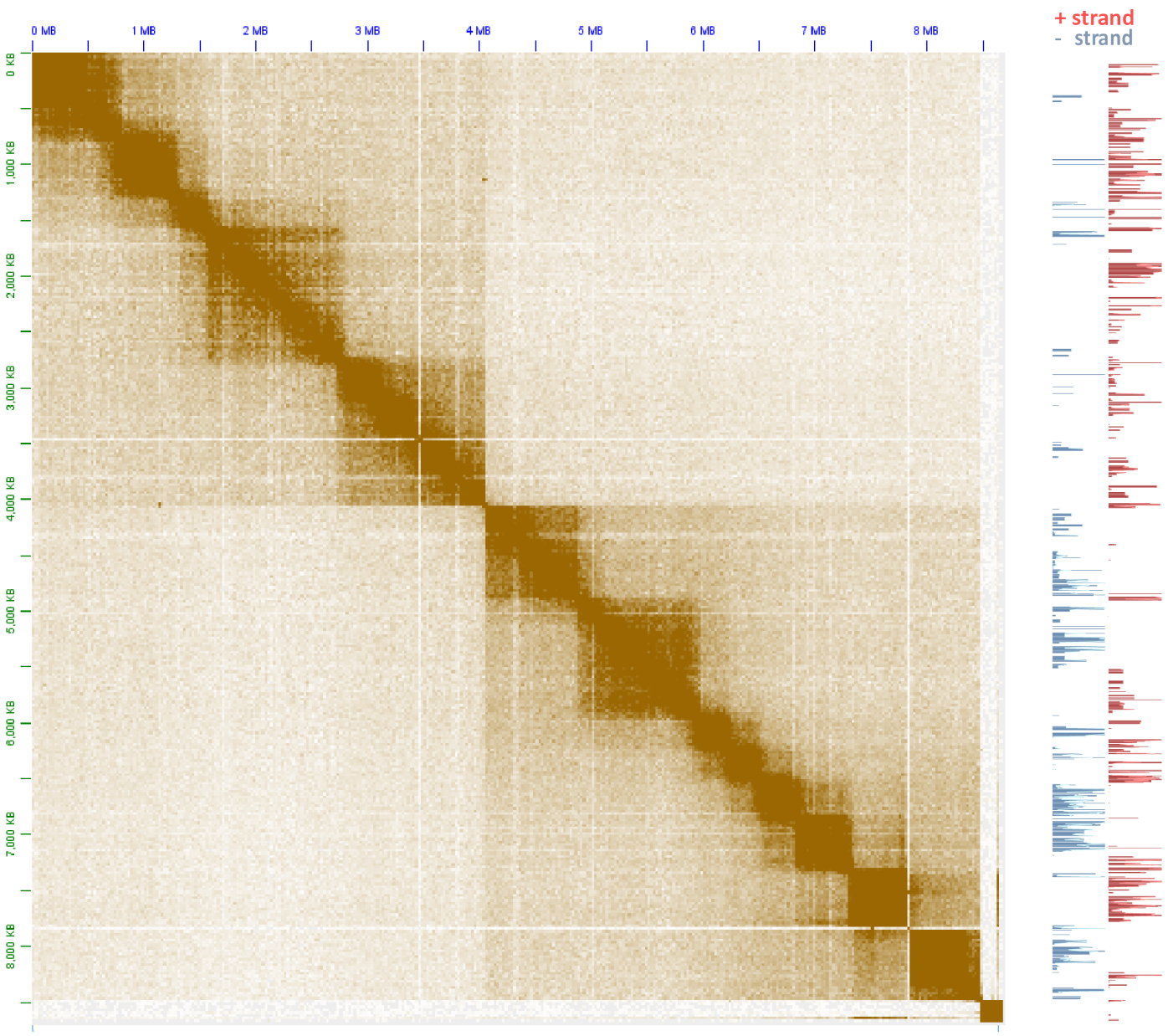

Supplementary Figure 13: The topological domain organization of dinoflagellate chromosomes is related to polycistronic gene array orientation. Shown is the 5kb-resolution KR-normalized Hi-C map together with strand-specific RNA expression levels for pseudochromosome 89.

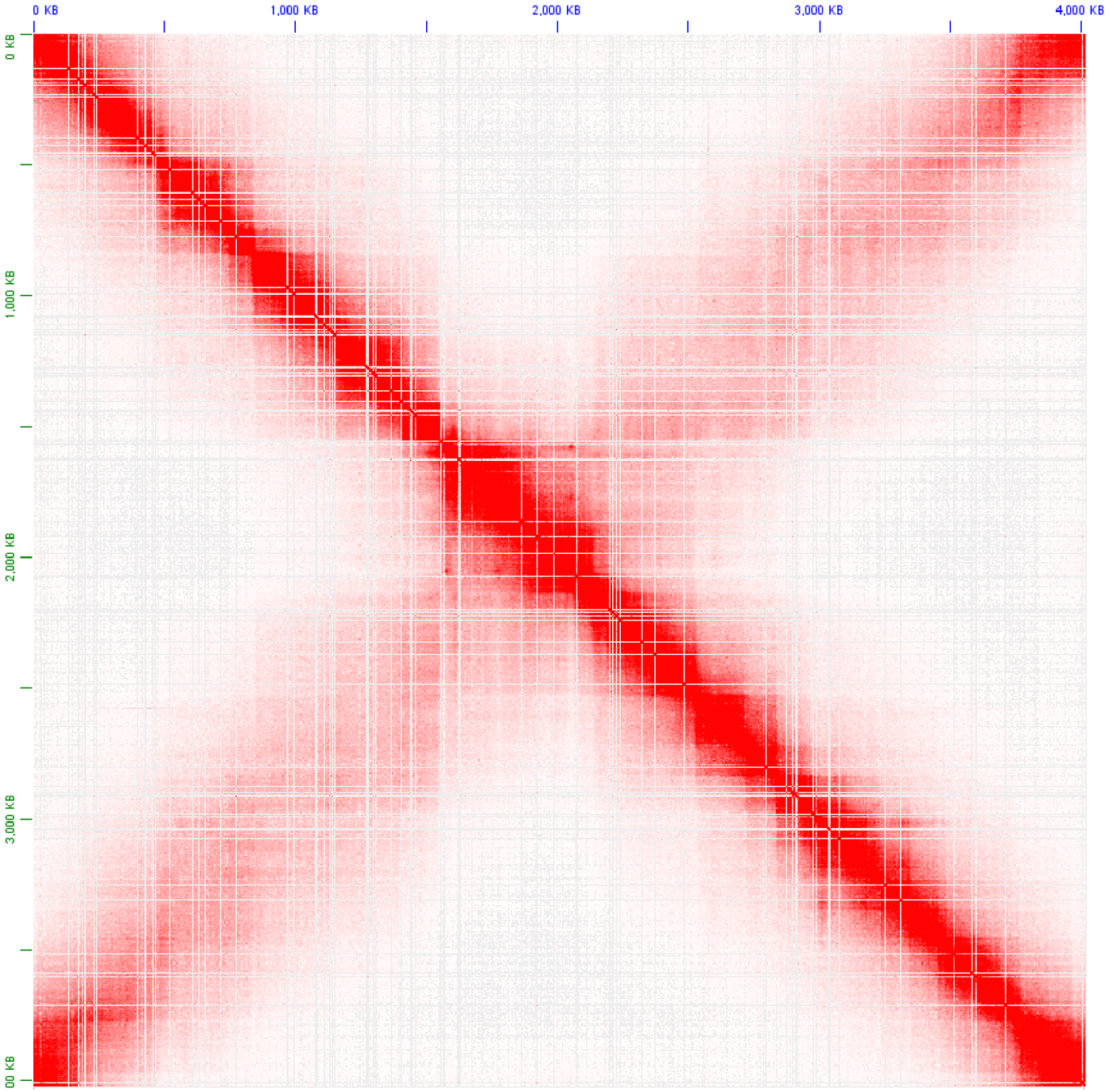

Supplementary Figure 14: Topological structure of the *Caulobacter crescentus* CB15 genome. Shown is the KR-normalized 5-kb resolution maps for the whole *Caulobacter* chromosome (GEO accession GSM1120448).

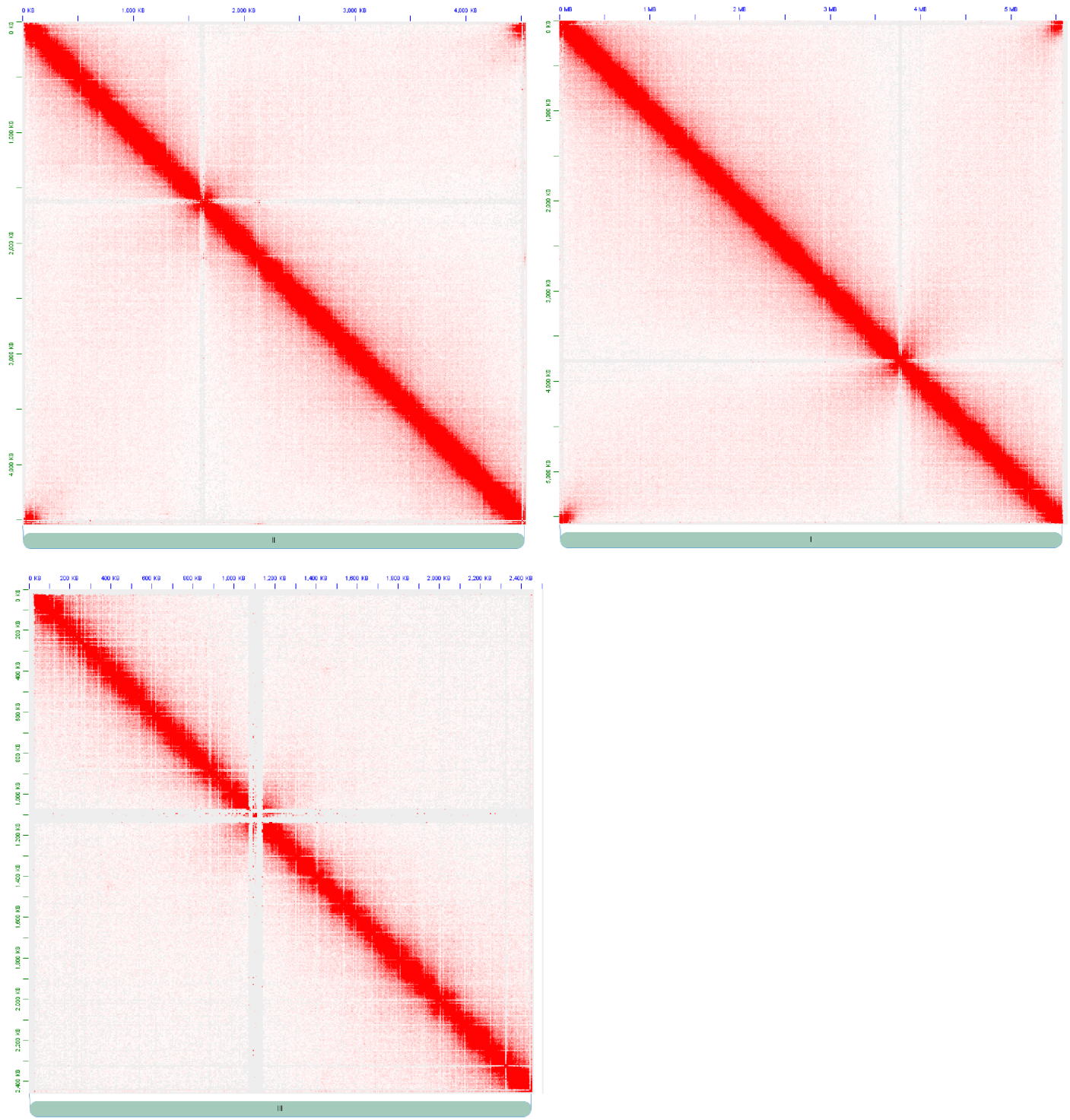

Supplementary Figure 15: Topological structure of the *Schizosaccharomyces pombe* genome. Shown are the KR-normalized 5-kb resolution maps for all three *S. pombe* chromosome (GEO accession GSM1379427).

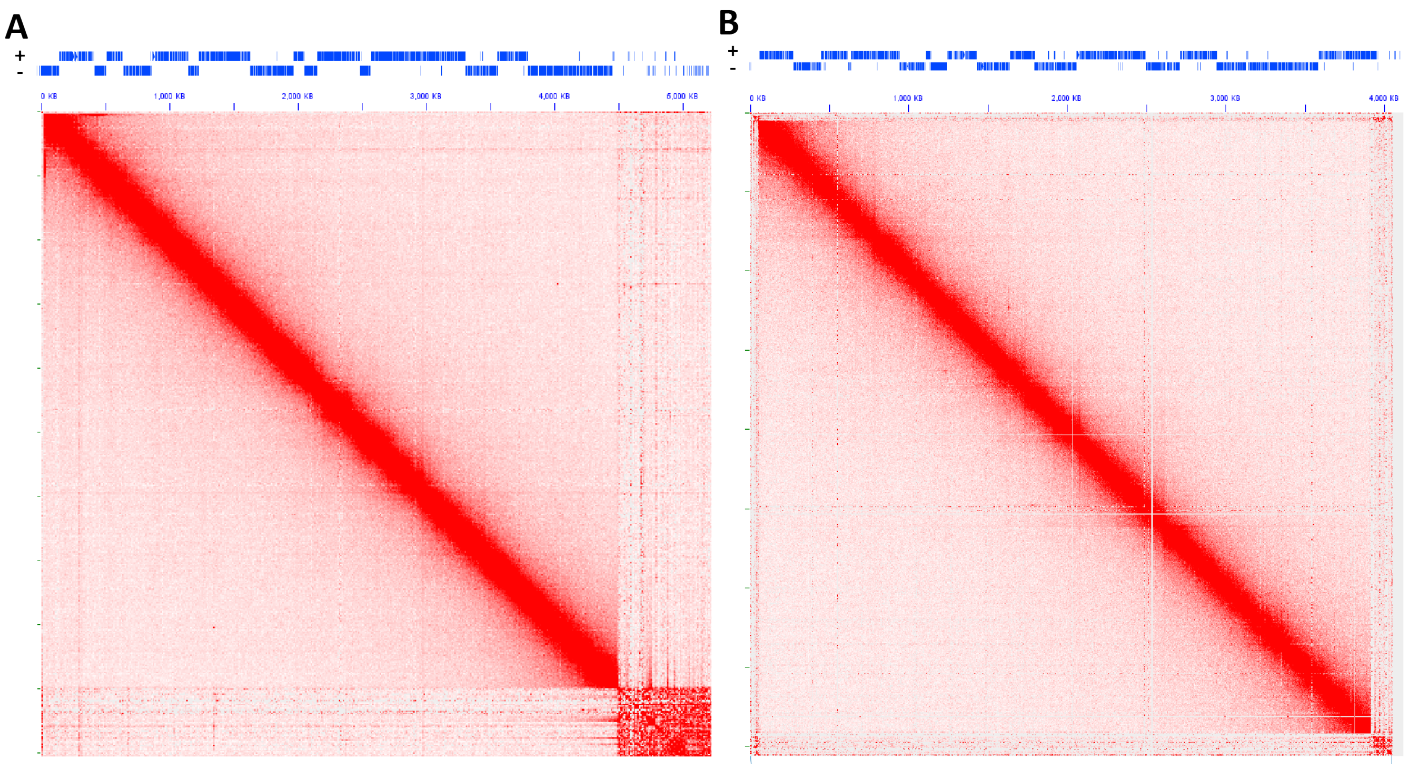

Supplementary Figure 16: No topological domains associated with gene arrays are observed in the kinetoplastid *Trypanosoma brucei*. Shown are KR-normalized 10-kb resolution maps for chr11 (A) and chr10 (B) for GEO accession GSM3346690.

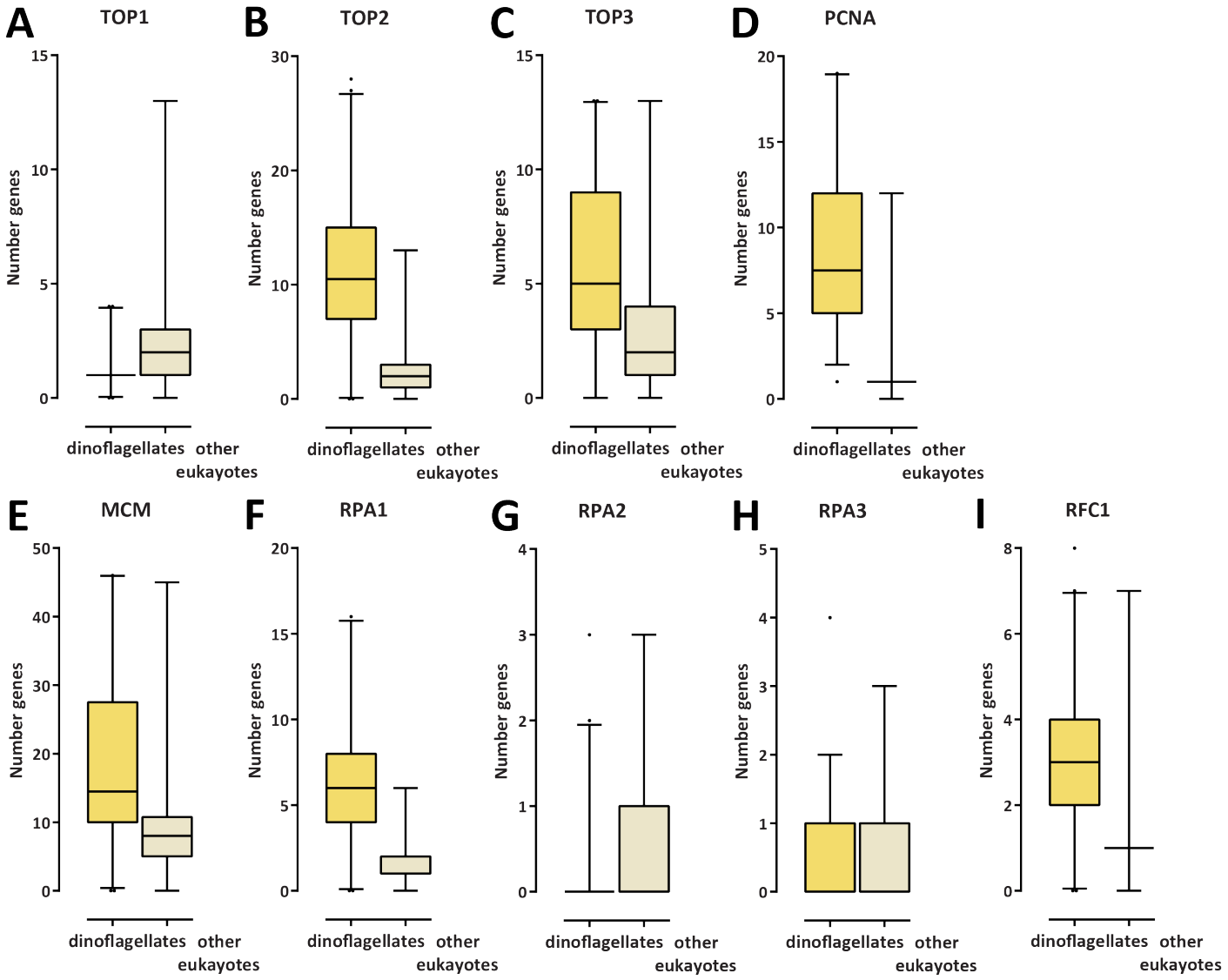

Supplementary Figure 17: Expansion of the Type II and II topoisomerase gene repertoire as well as of certain other replication-related proteins in dinoflagellates. Shown are the number of genes annotated in MMETSP transcriptome assemblies of dinoflagellates and other eukaryotes. (A) Number of Type I topoisomerase genes; (B) Number of Type II topoisomerase genes; (C) Number of Type III topoisomerase genes; (D) Number of PCNA genes; (E) Number of MCM genes; (F) Number of RPA1 genes; (G) Number of RPA2 genes; (H) Number of RPA3 genes; (I) Number of RFC1 genes.

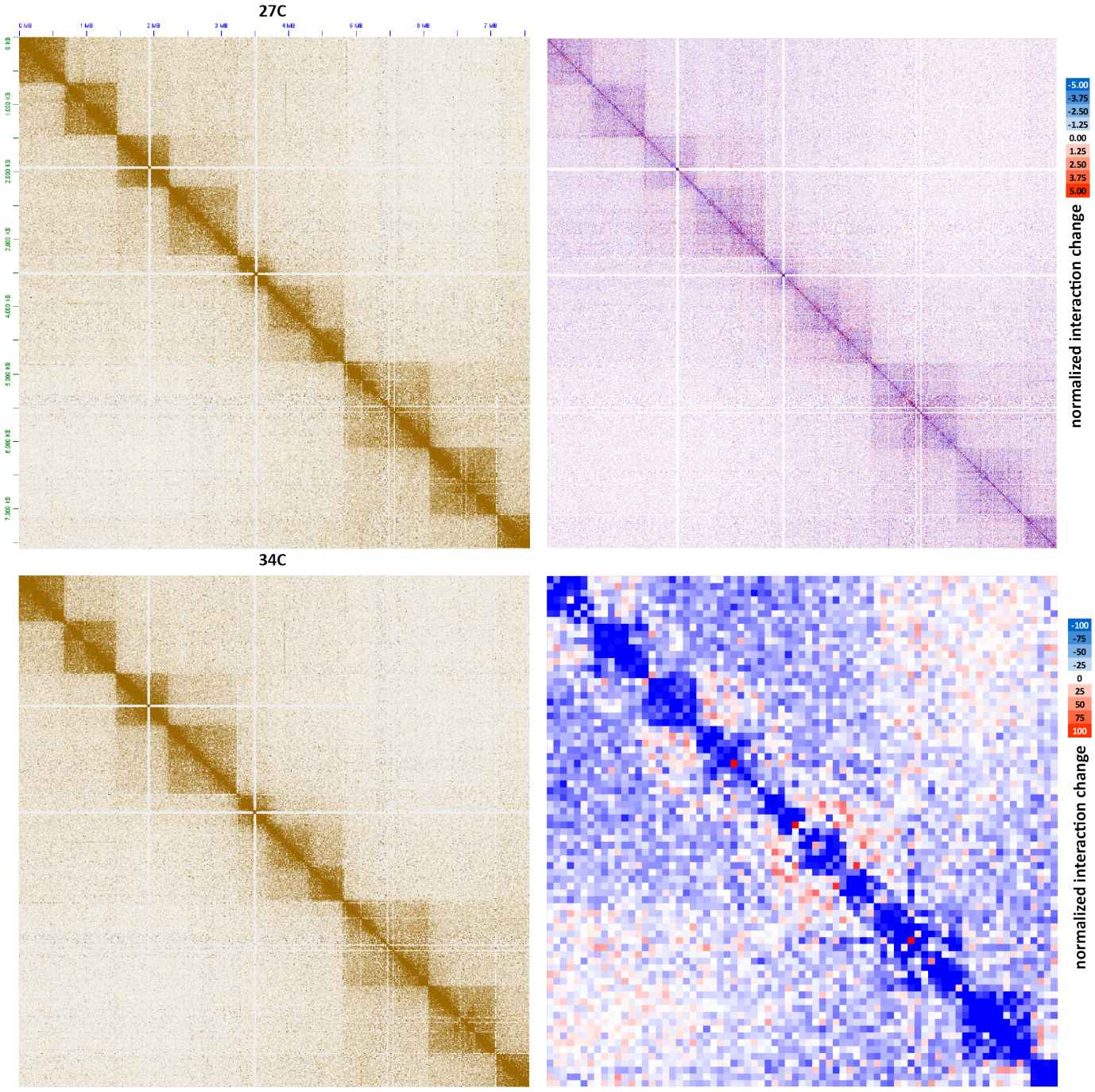

Supplementary Figure 18: Moderate decompaction of dinoTADs upon exposure to elevated temperatures. Shown is pseudochromosome 10 (KR-normalized) and the difference between the KR-normalized Hi-C maps generated from *B. minutum* grown at 34 °C and at 27 °C at 100-kb resolution (lower right) and 5-kb resolution (upper right).

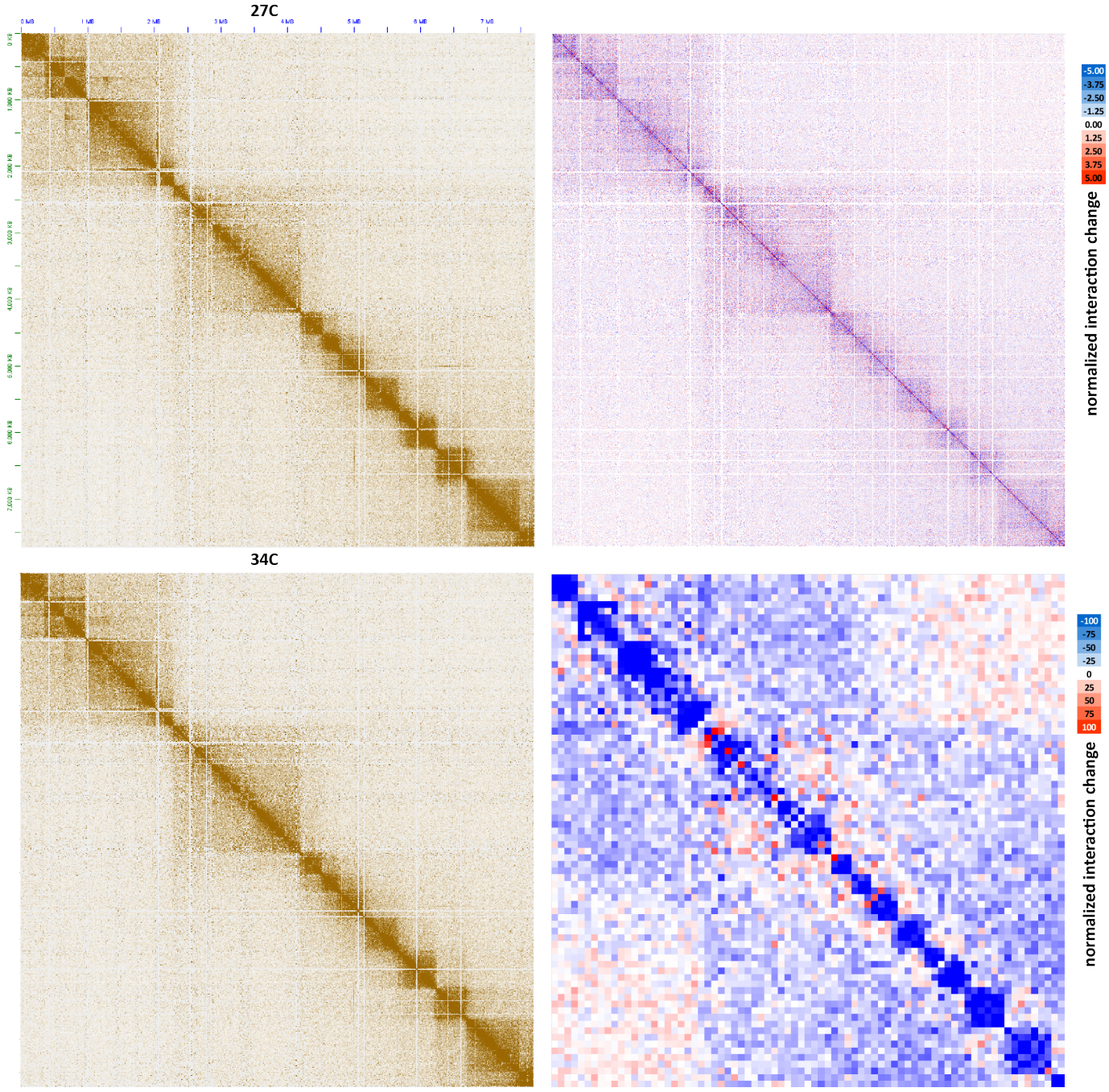

Supplementary Figure 19: Moderate decompaction of dinoTADs upon exposure to elevated temperatures. Shown is pseudochromosome 17 (KR-normalized) and the difference between the KR-normalized Hi-C maps generated from *B. minutum* grown at 34 °C and at 27 °C at 100-kb resolution (lower right) and 5-kb resolution (upper right).

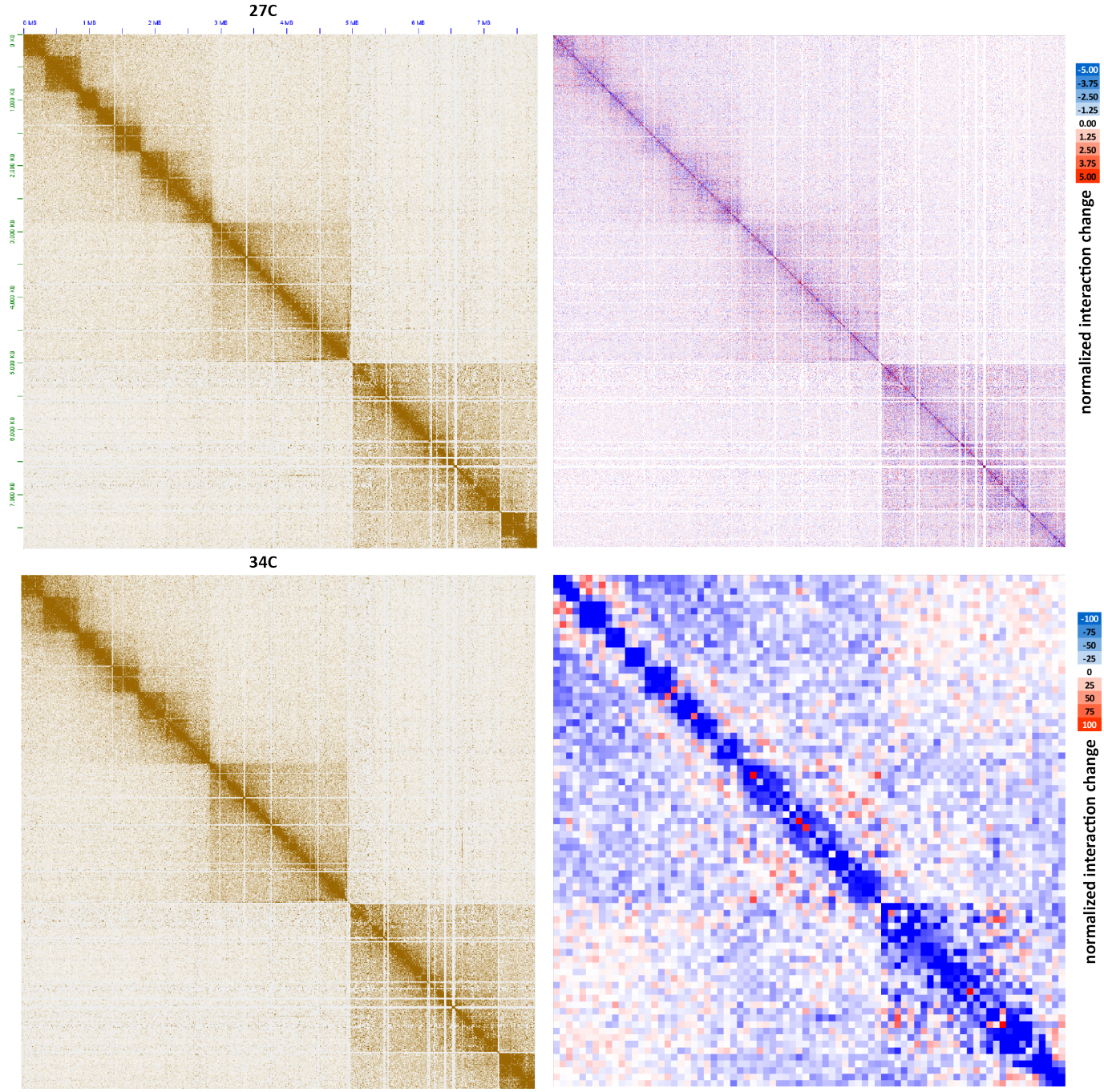

Supplementary Figure 20: Moderate decompaction of dinoTADs upon exposure to elevated temperatures. Shown is pseudochromosome 18 (KR-normalized) and the difference between the KR-normalized Hi-C maps generated from *B. minutum* grown at 34 °C and at 27 °C at 100-kb resolution (lower right) and 5-kb resolution (upper right).

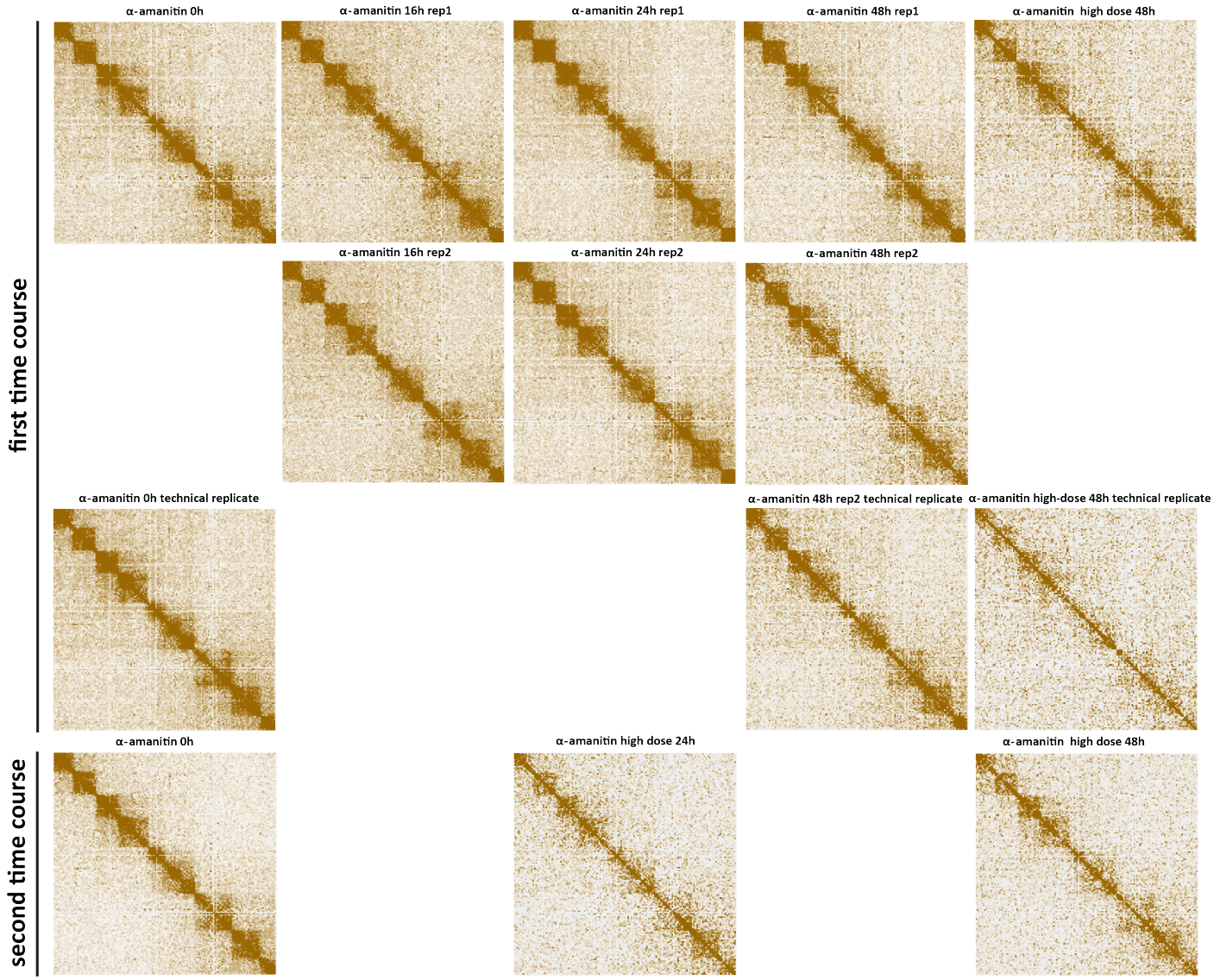

Supplementary Figure 21: Decompaction of dinoTADs upon transcriptional inhibition using α-amanitin. Shown is pseudochromosome 10. Two time courses were carried out following the outline presented in Figure 2B.

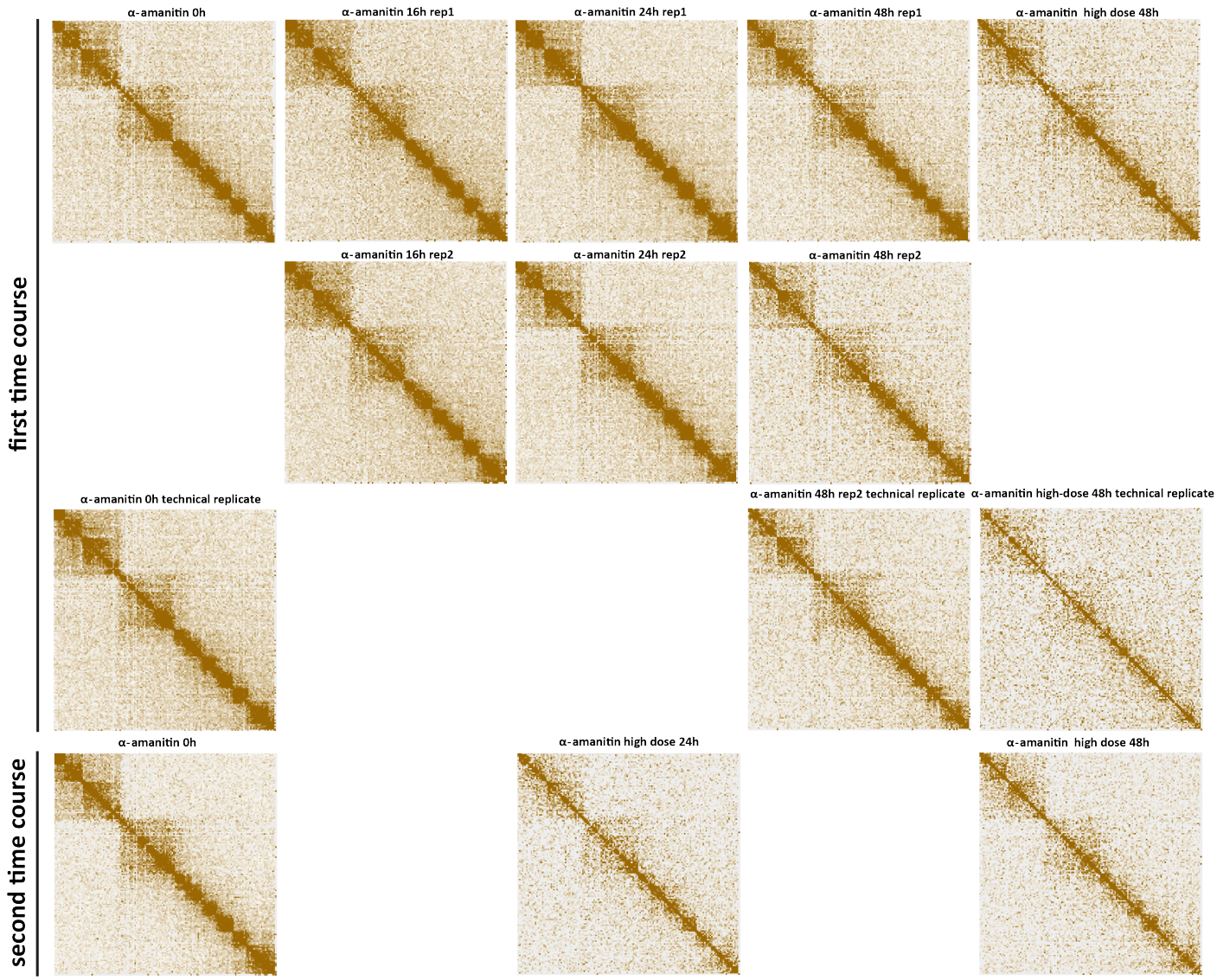

Supplementary Figure 22: Decompaction of dinoTADs upon transcriptional inhibition using α-amanitin. Shown is pseudochromosome 17. Two time courses were carried out following the outline presented in Figure 2B.

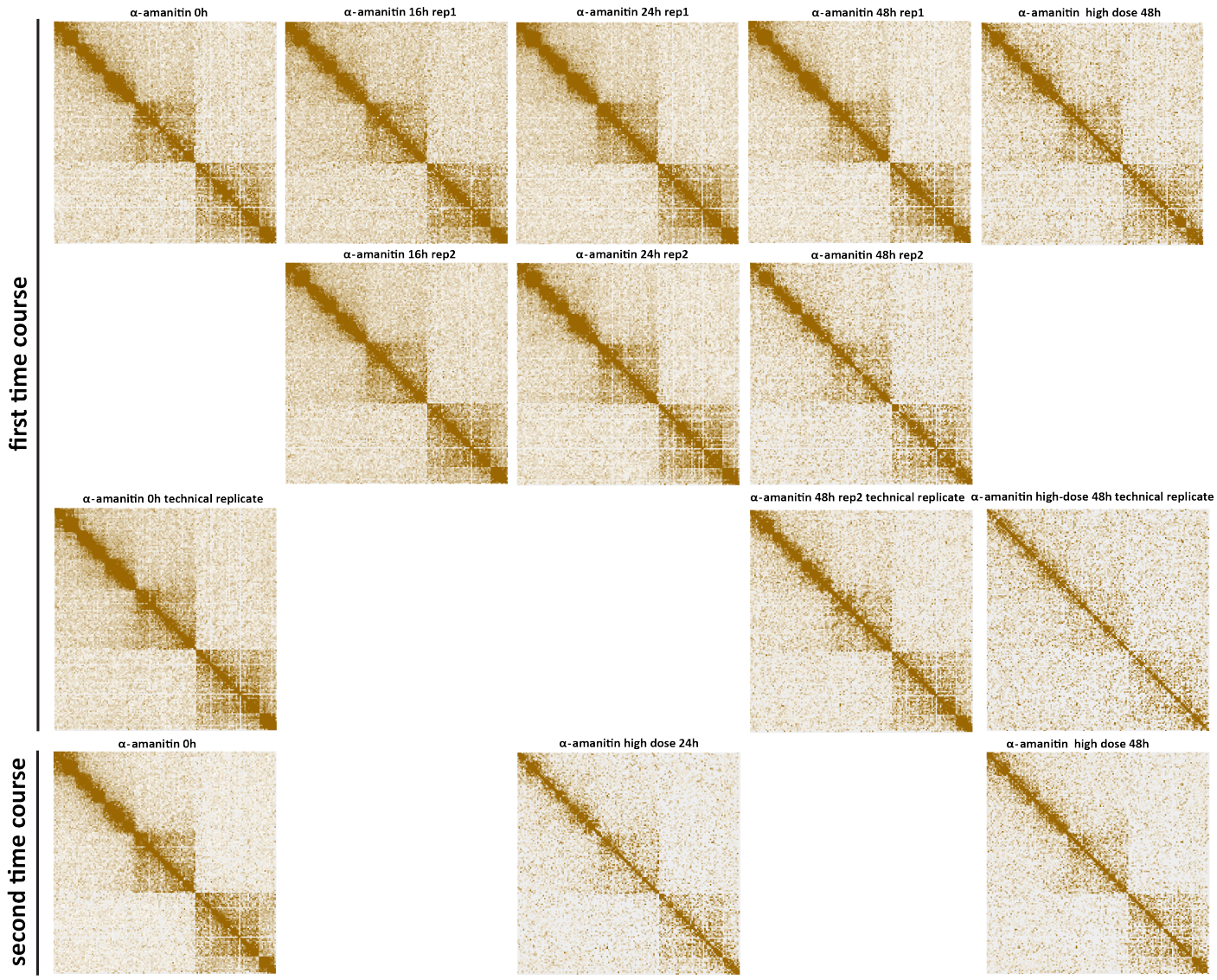

Supplementary Figure 23: Decompaction of dinoTADs upon transcriptional inhibition using α-amanitin. Shown is pseudochromosome 18. Two time courses were carried out following the outline presented in Figure 2B.

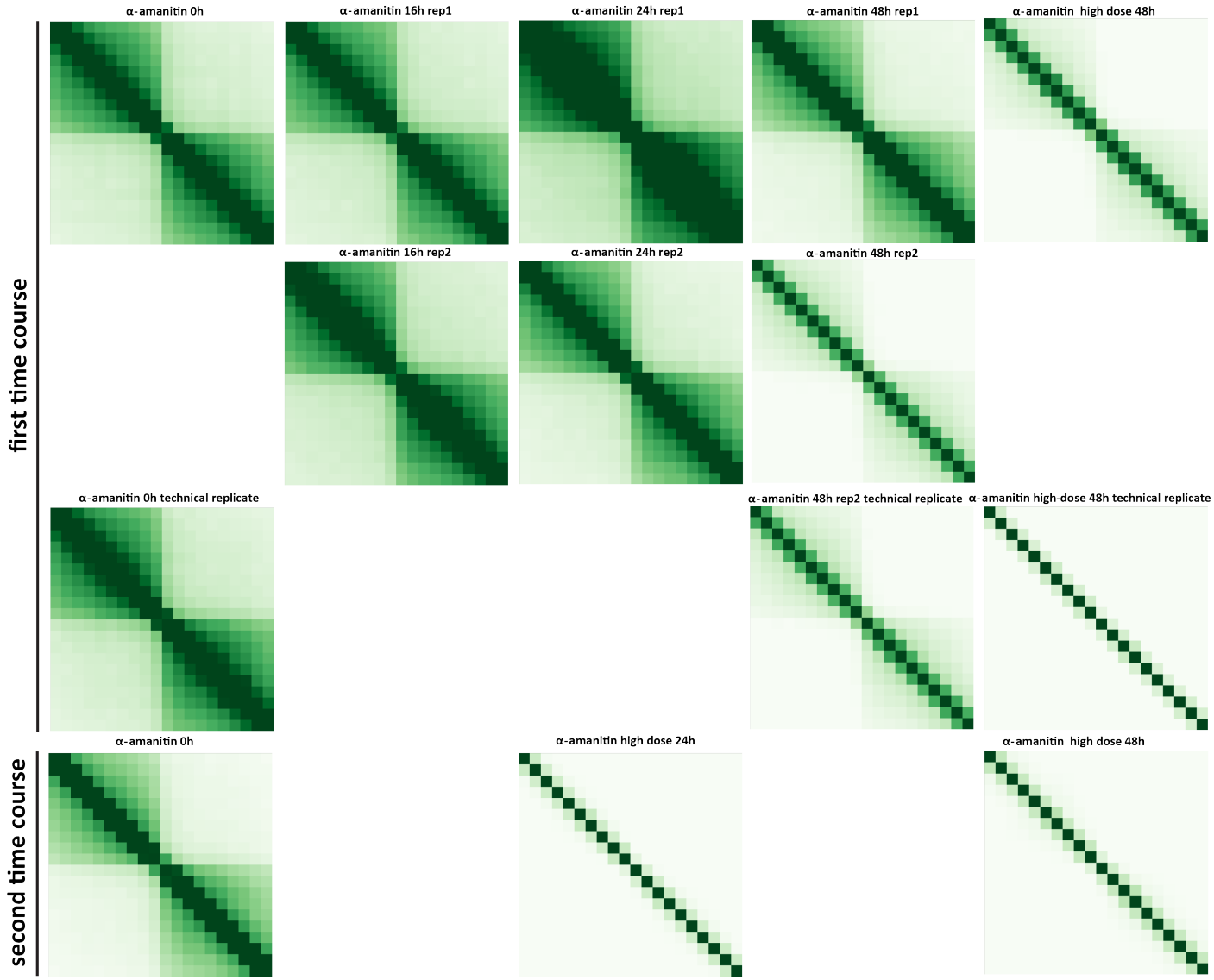

Supplementary Figure 24: Decompaction of dinoTADs upon transcriptional inhibition using α-amanitin. Shown are 50-kb resolution metaplots centered on dinoTAD domain boundaries. Two time courses were carried out following the outline presented in Figure 2B.

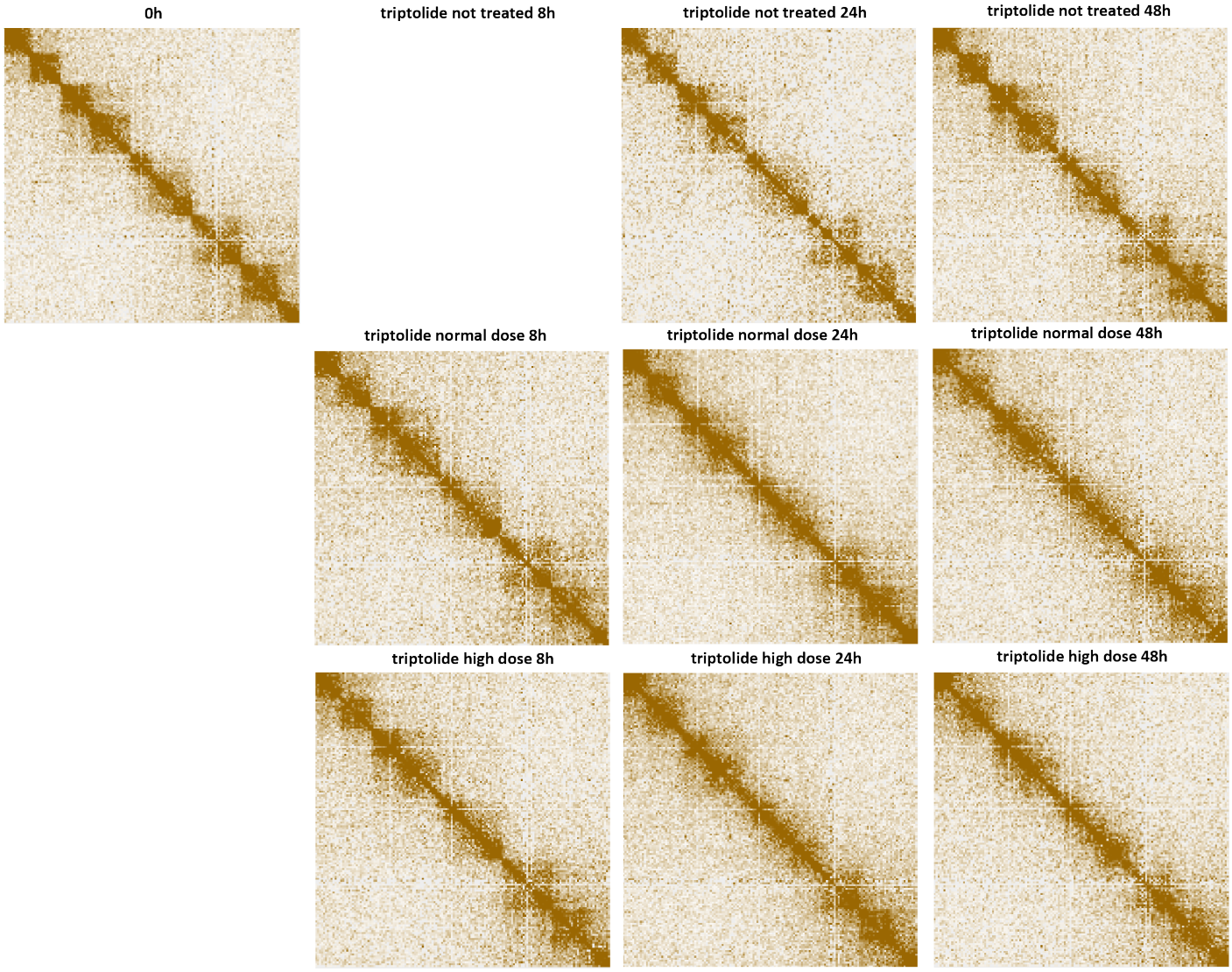

Supplementary Figure 25: Blurring of dinoTAD boundaries upon transcriptional inhibition using triptolide. Shown is pseudochromosome 10. The triptolide time course was carried out following the outline presented in Figure 2B.

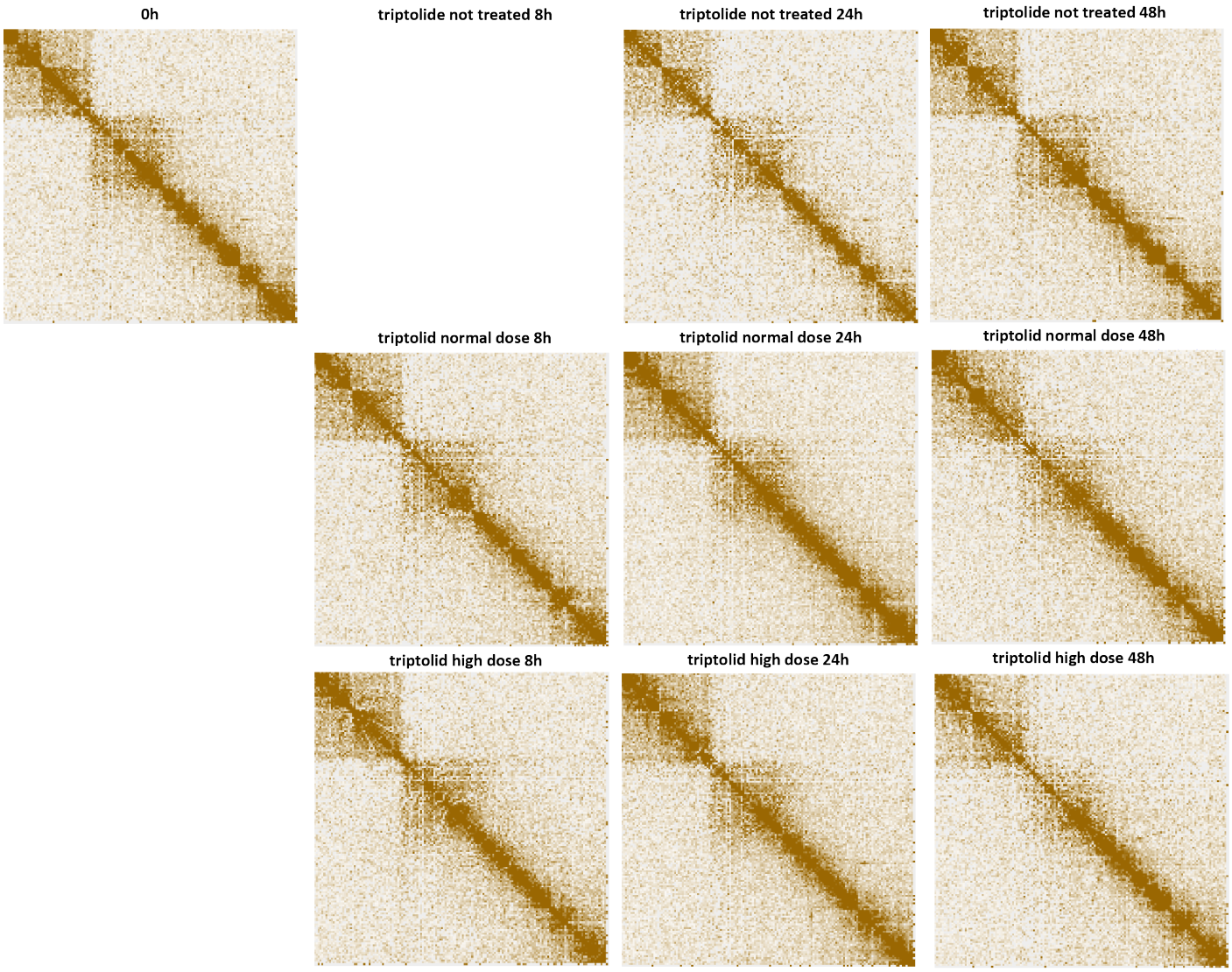

Supplementary Figure 26: Blurring of dinoTAD boundaries upon transcriptional inhibition using triptolide. Shown is pseudochromosome 17. The triptolide time course was carried out following the outline presented in Figure 2B.

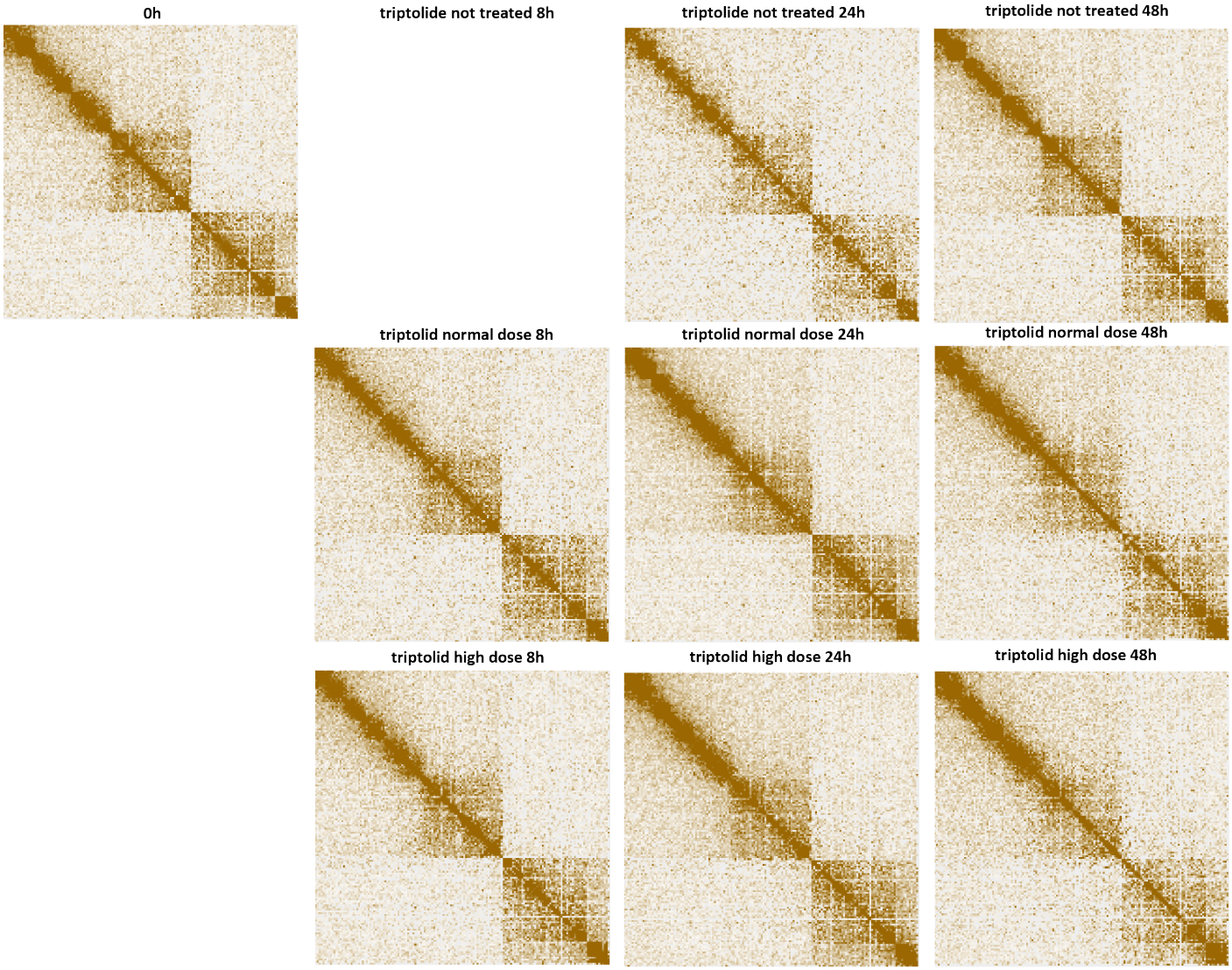

Supplementary Figure 27: Blurring of dinoTAD boundaries upon transcriptional inhibition using triptolide. Shown is pseudochromosome 18. The triptolide time course was carried out following the outline presented in Figure 2B.

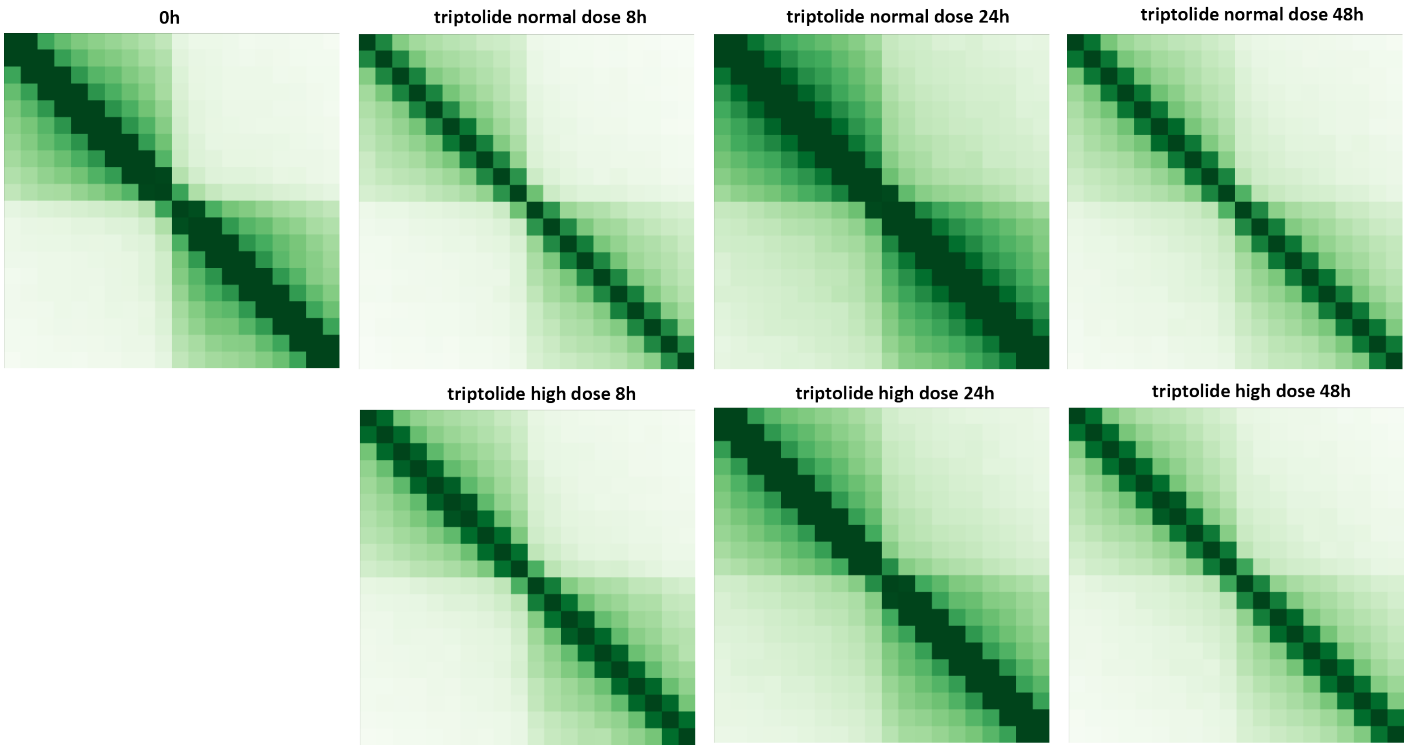

Supplementary Figure 28: Blurring of dinoTAD boundaries upon transcriptional inhibition using triptolide. Shown are 50-kb resolution metaplots centered on dinoTAD domain boundaries. The triptolide time course was carried out following the outline presented in Figure 2B.